50 YEARS of strain
strain
An International Journal for Experimental Mechanics

An Introduction to the Properties of Silica Glass in Ballistic Applications

S. M. Walley

SMF Fracture and Shock Physics Group, Cavendish Laboratory, J.J. Thomson Avenue, Cambridge CB3 0HE, UK

ABSTRACT: The purpose of this review is to introduce the interested reader to the literature on the use of silica glasses in ballistic applications. These applications include optically transparent windows (where their amorphous nature, appropriate band gap, and cheapness make them ideal window materials) as well as layers in opaque armours designed to be resistant to shaped charges. In the latter application, their increase in volume (bulking) on fracture disrupts the shaped charge jet. Other topics covered in this review include low-velocity damage by windborne debris, liquid and solid impact, dynamic methods of testing (Hopkinson pressure bar, Taylor impact, and plate impact shock loading), and constitutive models. The use of glass as a shaped charge is also discussed.

KEY WORDS: *ballistic, constitutive, fragmentation, glass, hypervelocity, modelling, shaped charge, shock, silica*

1. Introduction and Some Observations

Silica-based glasses may seem unlikely materials to be used in armours as in daily life it is the archetypal brittle material. Indeed, its response to debris picked up by hurricane-force winds [1–5] or to blast from terrorist bombs [6–16] is a major concern. Glass plates have long been known to deflect bullets fired through them at an angle [17–21]. The first study I have been able to find on the interaction of a bullet with a sheet of glass was published in 1927 [22].

Including a layer of glass within an opaque armour significantly increases an armour's resistance to the fastest projectile it is possible to launch artificially, namely shaped charges [23–30]. This is often attributed to the phenomenon of 'bulking' in which a fractured brittle material occupies a larger volume than it did before it was damaged [24, 26, 28, 29,31, 32].

The application of a thin polymer film to the rear of a glass window improves safety [33]. Also, lamination of glass with transparent polymer layers allows vehicle windshields or windows in buildings to withstand low-velocity impact without shattering [2, 34–42]. Thicker versions are used in armoured vehicles to make them proof against even high-velocity rifle bullets [43–48].

The only alternative for armoured windows at the moment is fine-grained polycrystalline AlON [49–58]. Silica glass, however, is intrinsically transparent due to its amorphous structure and appropriate band gap [59].

2. Methods of Studying the Dynamic Properties of Glass

In order to understand and be able to model the processes that occur when glass is ballistically impacted, it is necessary to know the dynamic properties of glass. Over the years, a number of techniques have been developed to do this, some of them adapted from the study of ductile materials [60].

(a) High-speed photography

As cracks in glass propagate at velocities of km s^{-1}, high-speed photography is invaluable in these studies [61–64]. From Figure 1, it is clear that cracks propagate more slowly than elastic waves. This means that in a finite body, the compressive elastic waves generated by impact have time to reflect off free surfaces as tensile elastic waves and return to interact with the growing cracks (Figure 2) by reducing the compressive component of the stress field, and even perhaps altering the stress in certain directions and places to tensile. Where this happens, faster crack growth will occur, which, if fast enough, may lead to bifurcation (see Figure 2). Bifurcation can also be caused by forcing cracks to grow fast by external constraint [62, 65–69] or by locked-in internal stresses such as those existing in thermally toughened glass [70, 71] and Prince Rupert's drops [71–76].

(b) Split Hopkinson pressure bar

The split Hopkinson pressure bar (SHPB) was originally developed in the 1940s for the measurement of the high-rate flow stresses of ductile materials such as polymers [78, 79] and metals [80]. Ductile materials can be tested this way under conditions of one-dimensional stress (unconfined), but brittle materials such as glass are usually confined by a metal sleeve (Figure 3) during dynamic deformation in an SHPB [81–84]. The reason for using a sleeve is that brittle materials fracture before stress equilibrium is achieved. The sleeve holds the pieces together so that load can be measured, but in a state of one-dimensional strain rather than one-dimensional stress.

Nie and co-workers [82, 84] reported a double-pulse SHPB technique (Figure 4) where the duration of the first load can be controlled using a momentum trap positioned at various distances from a flange on the impact end of the incident

P/C Ex 133

© 2013 Wiley Publishing Ltd
doi: 10.1111/str.12075

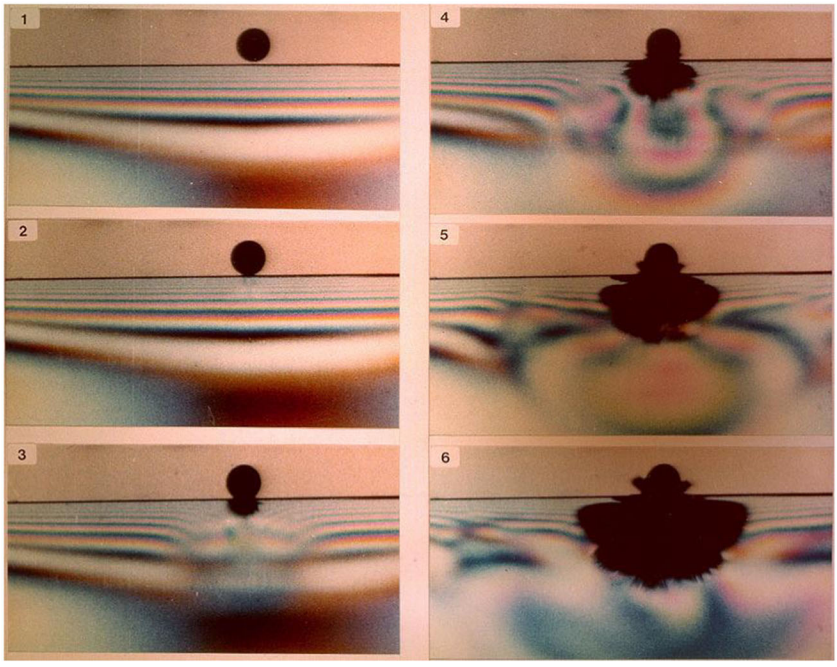

Figure 1: High-speed photographic sequence (1 μs interframe time) of the impact of a 2-mm-diameter tungsten carbide ball onto toughened glass at 150 m s^{-1}. The stress pattern was visualised using a photoelastic arrangement for observing isochromatics. From [77]

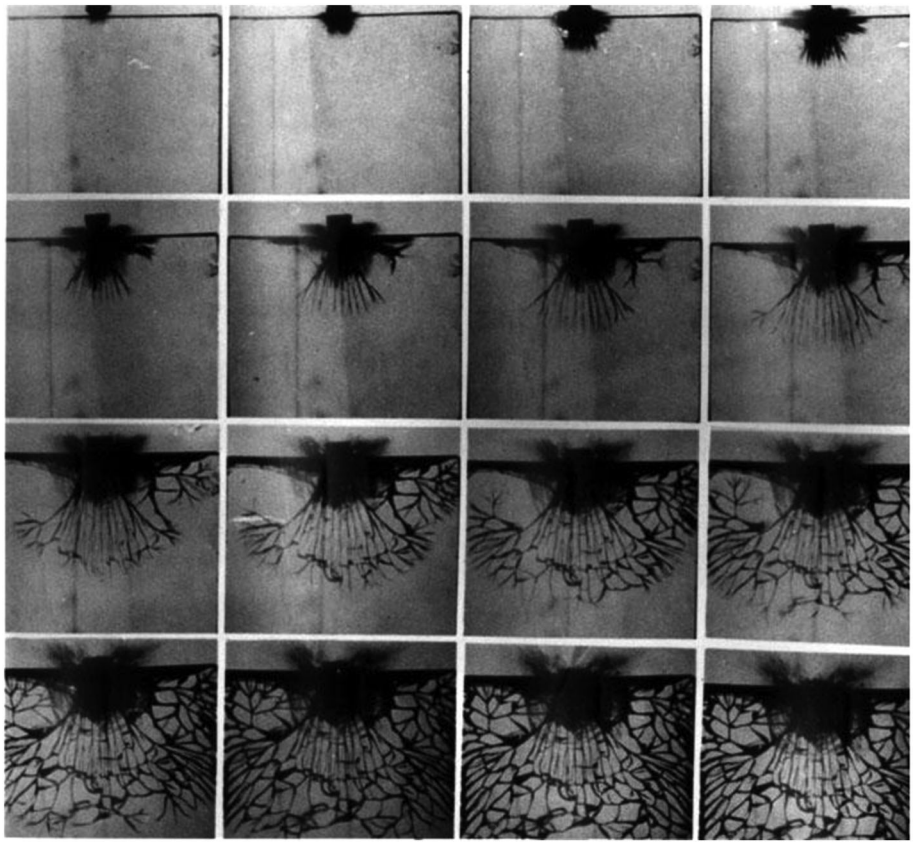

Figure 2: Fracture propagation in a 50 × 50 × 6.2-mm sheet of toughened windscreen glass after impact with a lead airgun pellet at the top. Interframe time 2 μs. From [70]

© 2013 Wiley Publishing Ltd
doi: 10.1111/str.12075

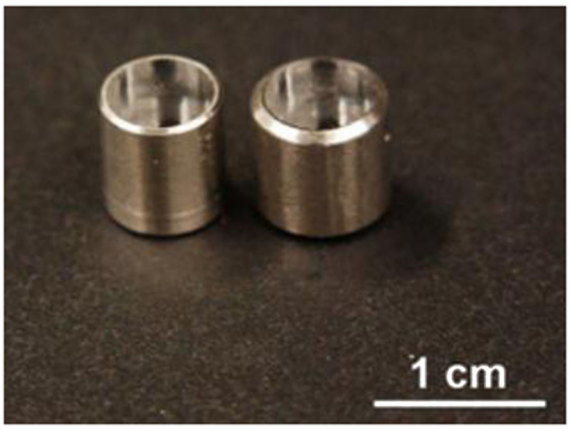

Figure 3: Examples of stainless steel sleeves used to confine glass cylinders for dynamic testing in a split Hopkinson pressure bar. From [84]

bar (Figure 5). This allows the damage state of the glass to be investigated at various points along the dynamic loading curve (Figure 6). They also showed that the dynamic strength–pressure relation for fully comminuted borosilicate glass was independent of temperature up to 600 °C (Figure 7).

(c) Taylor (or rod) impact

This technique was originally developed during the Second World War for estimating the dynamic compressive mechanical properties of metals [78, 85]. In its modern use for validating constitutive models, high-speed photography is used in order to follow the progress of the deformation [86, 87]. High-speed photography is essential if relaxation occurs after impact such as occurs with polymers [88]. But it is also necessary for brittle materials (such as ceramics and silica glasses) as there is no deformed cylinder to recover after the experiment [89–96]. Note that fracture propagation along glass bars induced by other types of loading has been studied by a number of authors [97–104].

At present, the only data obtainable from the Taylor test for validating constitutive models for both brittle and ductile materials are (i) the specimen profile as a function of time [86, 87,93] (see also Figures 8 and 9) and (ii) post-test examination of void growth and other damage [105]. However, it is possible that various X-ray techniques may soon provide data on internal damage mechanisms *as they are occurring*.

Note the very different behaviour of two types of glasses in Figures 8 and 9. Although both glasses behave in a brittle manner, becoming progressively opaque to light due to the creation of many internal fractures, the smooth external profile of the borosilicate rod looks like that of a ductile material. The profile of the soda-lime glass rod, however, is jagged with what looks like fragments jetting out periodically along the length of the rod away from the impact face. The reasons for the differences in the behaviour of the two glasses are not understood at present.

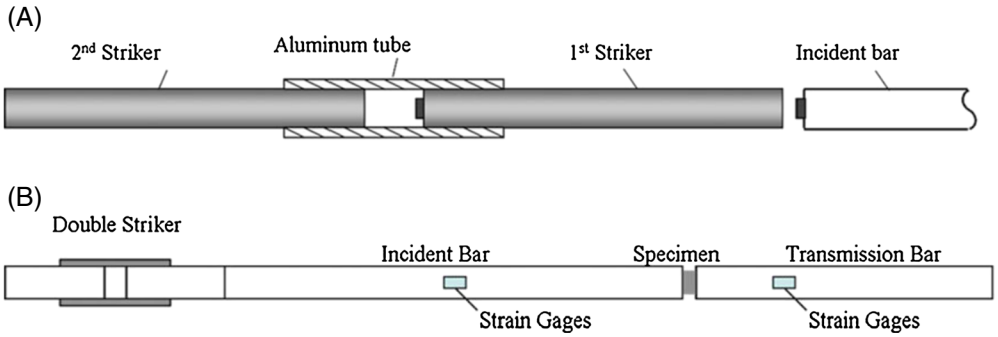

Figure 4: (A) Schematic diagram of the technique used to produce a double loading pulse in an split Hopkinson pressure bar; (B) schematic diagram showing the position of the glass specimen shown in Figure 3. From [84]

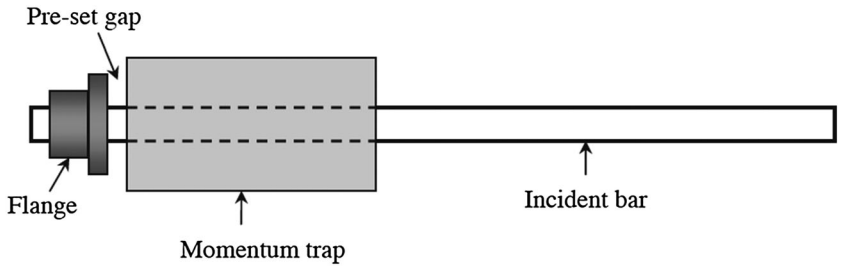

Figure 5: Schematic diagram of the momentum trap and flange arrangement at the impact end of the incident bar used for investigating the high-rate properties of silica glasses. From [84]

© 2013 Wiley Publishing Ltd
doi: 10.1111/str.12075

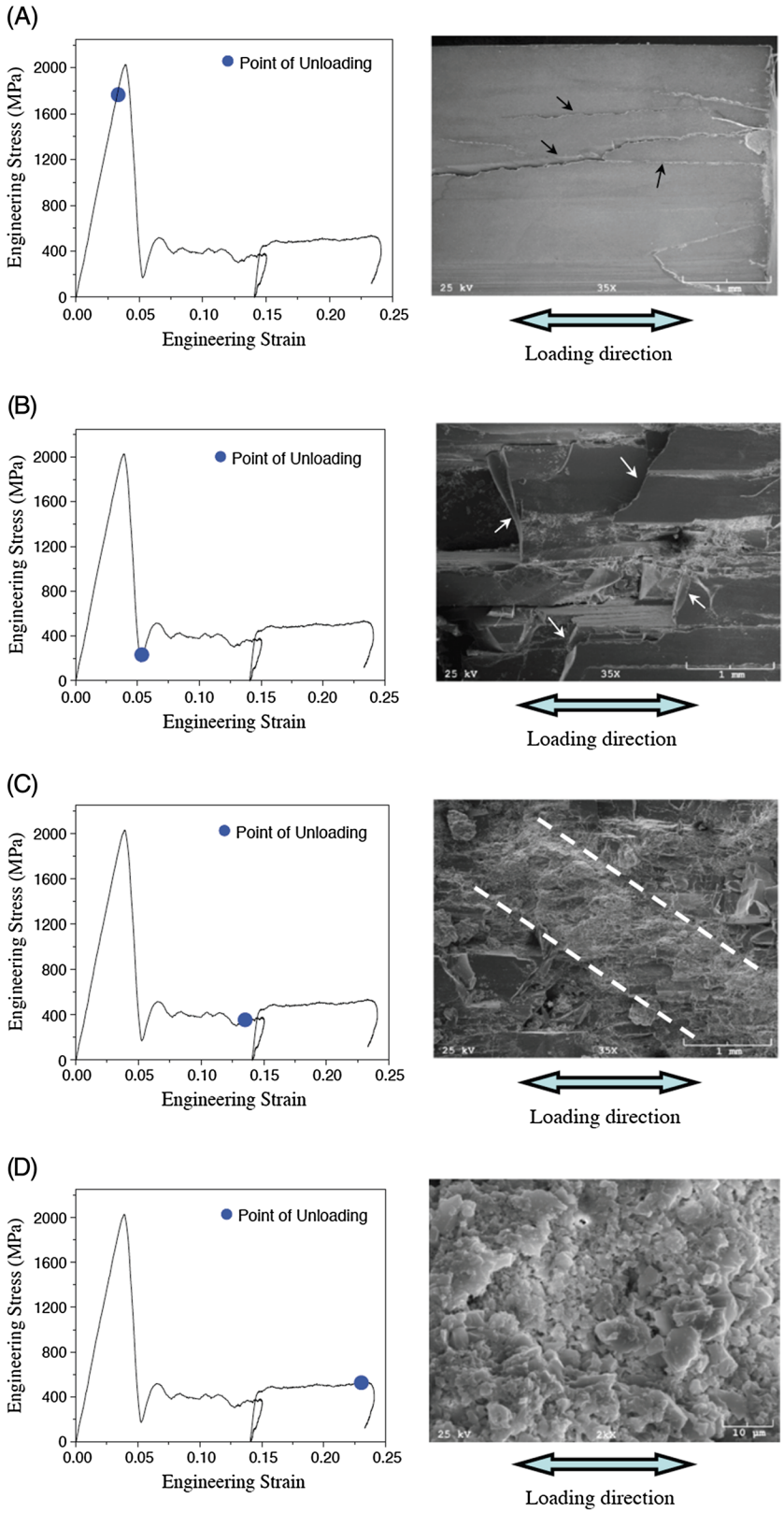

Figure 6: The development of damage in a borosilicate glass loaded dynamically using the split Hopkinson pressure bar apparatus shown schematically in Figures 4 and 5. From [84]

© 2013 Wiley Publishing Ltd |
doi: 10.1111/str.12075

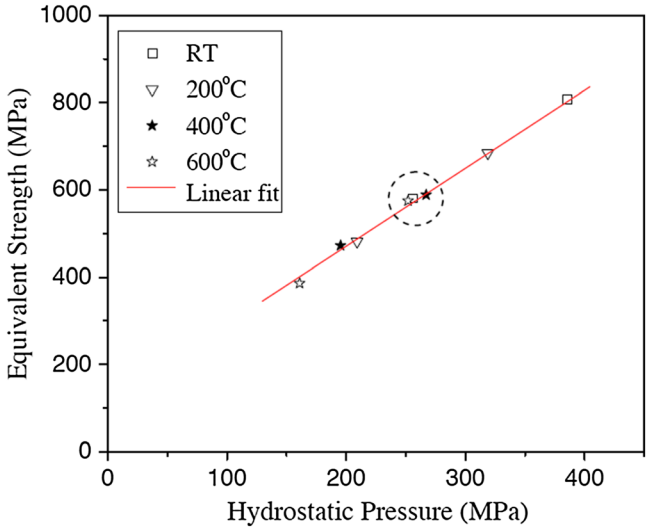

Figure 7: Plot of the strength–pressure relation for borosilicate glass tested dynamically at a strain rate of $900\,s^{-1}$ at three different temperatures in the split Hopkinson pressure bar apparatus shown schematically in Figures 4 and 5. From [84]. RT, room temperature

(d) Plate impact shock loading

Accurate measurements of the shock properties of materials started during World War 2 in connection with the Manhattan Project [106]. Initially, shocks were driven into materials using explosive charges, and a few papers on glass have been published using this technique, e.g. [6, 107–113]. In recent years, most such studies of glass have been performed using light gas guns [114], although explosive lenses are still used in shock studies where it is desired to control the rise (or ramp) time of the shock wave [115]. Brittle materials have been found to have a variety of responses to shock: some are relatively undamaged by shocks above their Hugoniot elastic limit (HEL), and others fail immediately after the HEL is exceeded. As with the SHPB, double-shock techniques can allow these matters to be resolved as it uses one shock to damage the material and a second shock immediately following to probe the state of the shocked material, particularly the shear and spall strength [116]. Rosenberg *et al*. [117] concluded that the HEL marks the point at which cracks coalesce into a network. Borosilicate glass has been shown to exhibit no loss of spall strength up to the HEL and then a substantial loss of shear strength when shocked above the HEL [118]. Soda-lime glass, on the other hand, shows a finite (though reduced) shear strength [119]. This loss of shear strength was correlated with a sudden increase in penetration depth at a certain critical impact speed [120] (see also Figure 10) when glass specimens were struck by flat-ended projectiles.

A stir was caused in the Shock Physics community when some Russian researchers showed that failure in shocked glass propagates some distance *behind* a compressive shock [121, 122] (see also Figure 11A). This phenomenon is often termed 'failure wave', but since, strictly speaking, it is not a wave, the term 'failure front' would be better [123]. The phenomenon was detected since the reload signal in the shock wave was smaller than would be expected than if a spall plane opened up in a previously undamaged material (compare Figure 11B and C). The Russian researchers interpreted the small reload signal to the existence of a region in the material with a finite shock impedance lower than the original material. Since the shock wave had had time to reflect off the back surface of the specimen and also be partially reflected off this zone of lower impedance, the failed zone must have been propagating more slowly than the shock wave velocity.

This paper resulted in a number of studies being carried out into this phenomenon in a number of laboratories [91, 114, 124–148]. High-speed photographic sequences of it occurring in glass have been obtained [130, 134]; see also Figure 12. Note in particular that the appearance of the failure front in the two glasses is very different. Strain gauge measurements have shown that soda-lime glass shocked above its HEL does not release back to zero strain (Figure 13), implying that densification or compaction of the glass has occurred.

As the shock pressure is raised, the gap between the failure front and the shock wave decreases, reaching zero at some critical impact shock pressure [135]. This immediately raises the issue of the kinetics of damage. It should be emphasised that failure fronts are only detectable photographically when the cracks have opened up to a separation greater than $\lambda/2$ (where λ is the wavelength of the illuminating light). Stress gauges are useful here in detecting any loss of shear strength in the material in the transparent region between the shock wave and the failure front.

Strain gauges can only measure strain where they are located and cannot distinguish between compressions (or dilations) of the glass on the atomic scale and on the mesoscale due to fracture (bulking). A thorough study of densification in explosively shocked glass was performed by Arndt and co-workers [111]. The parameter they used to assess densification was the refractive index of the resulting glass fragments. They measured this at various locations within the specimen and also as a function of applied shock pressure. They found that maximum densification occurred at the periphery of the impact face and minimum densification on the axis. They also found that there was an increase in density up to a shock pressure of 135 kbar followed by a decrease back to the unshocked value somewhere between 200 and 400 kbar. They attributed this to annealing due to the temperature rise induced by high-strength shocks. Cagnoux [150]

© 2013 Wiley Publishing Ltd
doi: 10.1111/str.12075

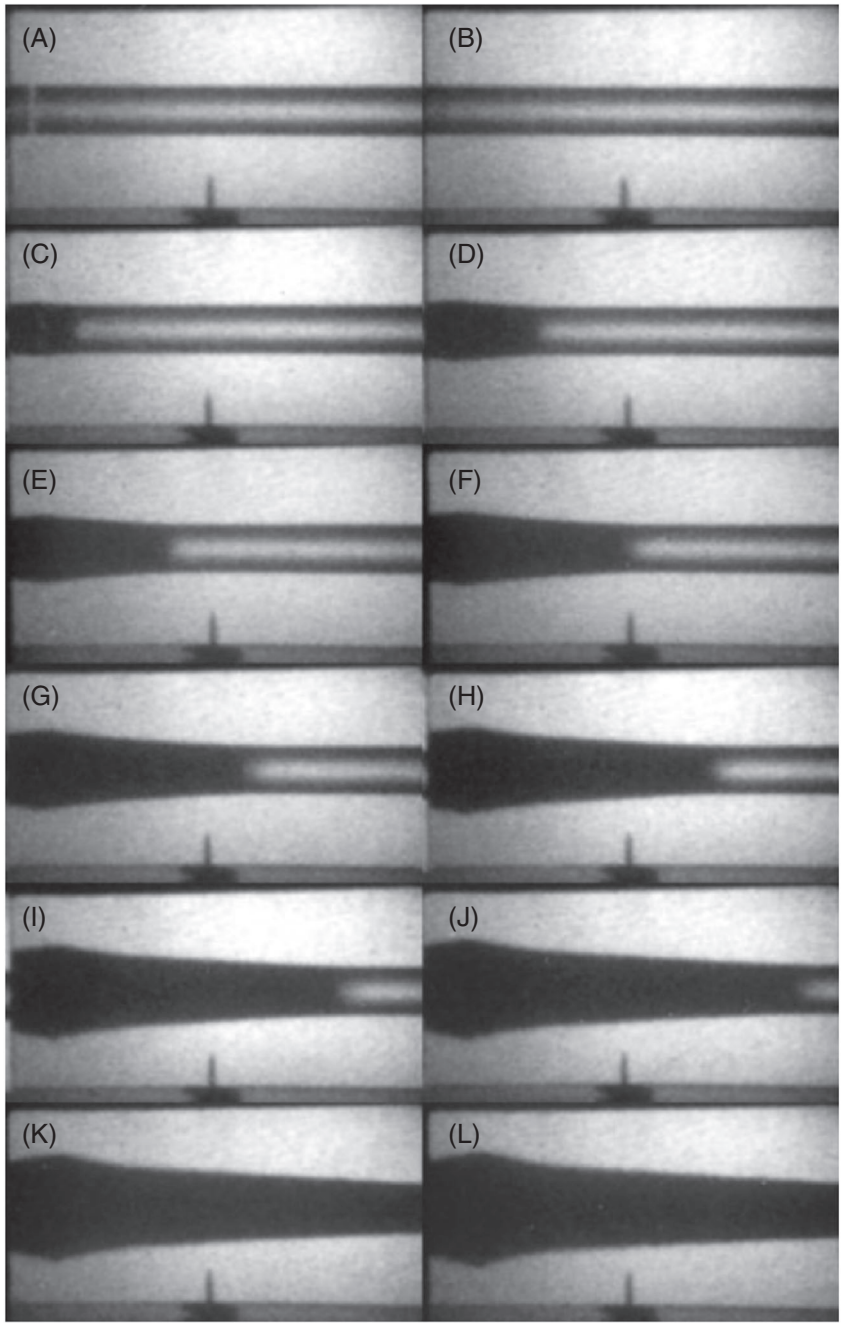

Figure 8: Symmetric Taylor impact of a borosilicate glass. Impact velocity 512 m s^{-1}. Rod dimensions: 10 mm diameter, 100 mm long. Interframe time 2 μs. An upturned drawing pin is included as a position marker. From [93]

observed that densification of glass reached a maximum for a shock strength of 170 kbar and was smaller for larger shocks. Densification of glasses under quasistatic high pressures was studied by Bridgman [151]. It has also been inferred in indentation experiments (Figure 14). A wide-ranging study of symmetrical explosive shocking of cylindrical specimens of silica and other brittle powders was performed by Deribas and co-workers [110, 152, 153]. They determined (amongst other things) the conditions under which silica powder can be fully densified to glass in this geometry.

Failure fronts have also been sought in other (opaque) brittle materials [127, 146, 155–158], although the evidence for their existence in materials apart from silica glasses is still controversial. Some researchers have claimed that in some brittle materials (such as alumina), failure does not propagate very far into the material from the impact surface [159–161], although others concluded this may

© 2013 Wiley Publishing Ltd
doi: 10.1111/str.12075

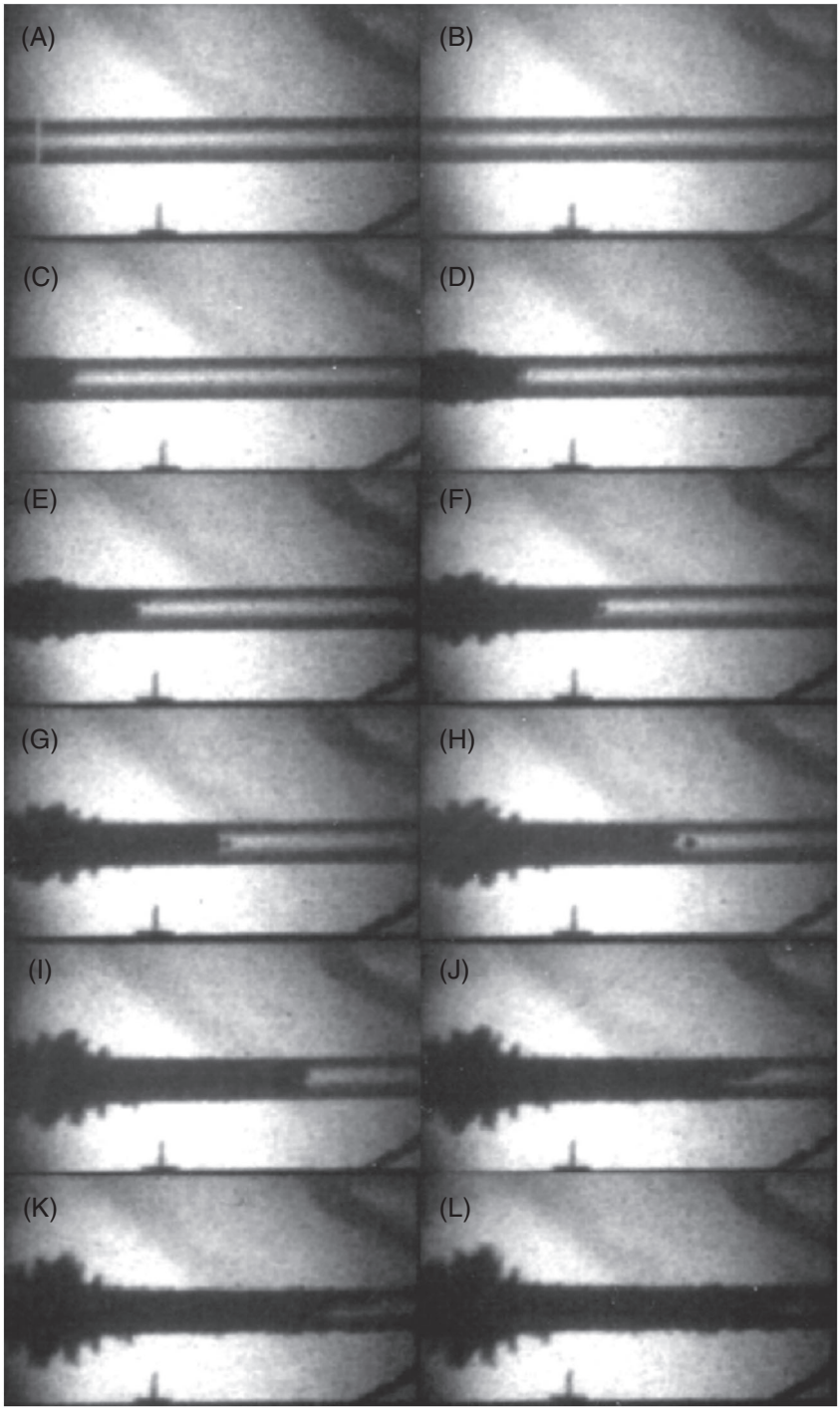

Figure 9: Symmetric Taylor impact of a soda-lime glass. Impact velocity 500 m s^{-1}. Rod dimensions: 10 mm diameter, 100 mm long. Interframe time 2 μs. An upturned drawing pin is included as a position marker. From [93]

be a measurement artefact [162, 163]. A few researchers have linked failure fronts to resistance to ballistic or hypervelocity impact [146, 147,155, 164–166]. Reviews of the failure front phenomenon have been written by Brar and Espinosa [126, 127].

An interesting observation to end this section on is due to Bourne and co-workers [114]. They found that the failed and unfailed shock shear stress glasses of widely differing densities lay on the same curves (Figure 15). Note that these data have *not* been scaled nor normalised. The origin of this behaviour

© 2013 Wiley Publishing Ltd
doi: 10.1111/str.12075

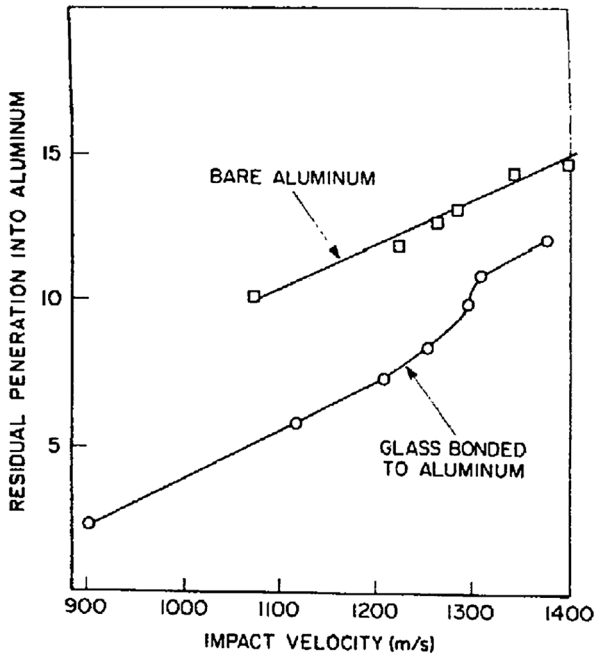

Figure 10: Graph showing the sudden increase in penetration depth at a critical speed for glass-faced aluminium. From [120]

is still uncertain but must lie in what the different glasses have in common: a random network of silicon dioxide tetrahedra.

A comparison of their data for glasses with armour ceramics is made in figure 16. They were able to relate the deviatoric response of brittle materials (including silica glasses) to their ballistic performance [168]. One important aspect of this phenomenon they missed, however, is the pressure dependence of the shear stress of the failed material (figure 17) [167]. This is simply because they did not perform experiments at high enough shock stresses. It would be expected that a comminuted material (i.e. a granular material) would obey a pressure-dependent yield criterion, although the arrangement of the grains will be different to that in, for example, a sand since in a fractured material the grains will be locked together until flow begins.

Progress is also being made at present into the molecular derivation of the Hugoniot and shock properties of glass [169–171].

3. Damage Mechanisms

Impacts of spheres on glass blocks at velocities ranging from a few $m\,s^{-1}$ to a few hundred $m\,s^{-1}$ often produces cone-shaped damage (see Figure 18). This is also characteristic of quasistatic indentation [172–180] (see Figure 19) and is explained by the cracks tending to follow trajectories of maximum tensile stress. These

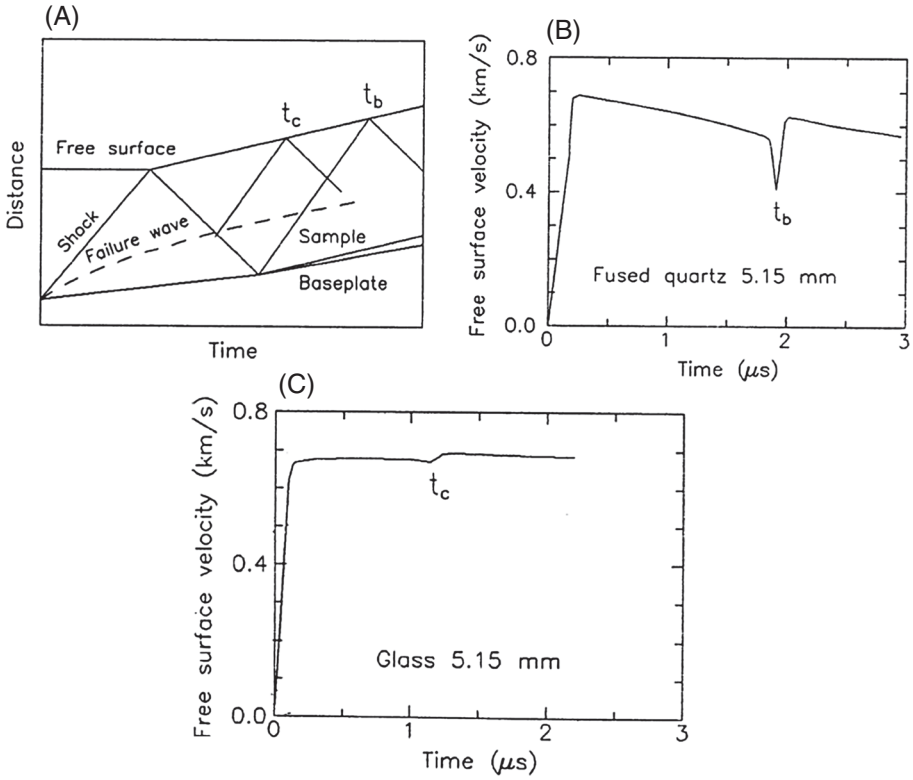

Figure 11: Original evidence for failure fronts. From [122]. (A) Schematic diagram showing effect of failure front on reflected shock wave; (B) expected reload signal if a spall plane opened up in undamaged glass; (C) reload signal (at time t_c) due to shock wave partially reflecting off failure front

© 2013 Wiley Publishing Ltd
doi: 10.1111/str.12075

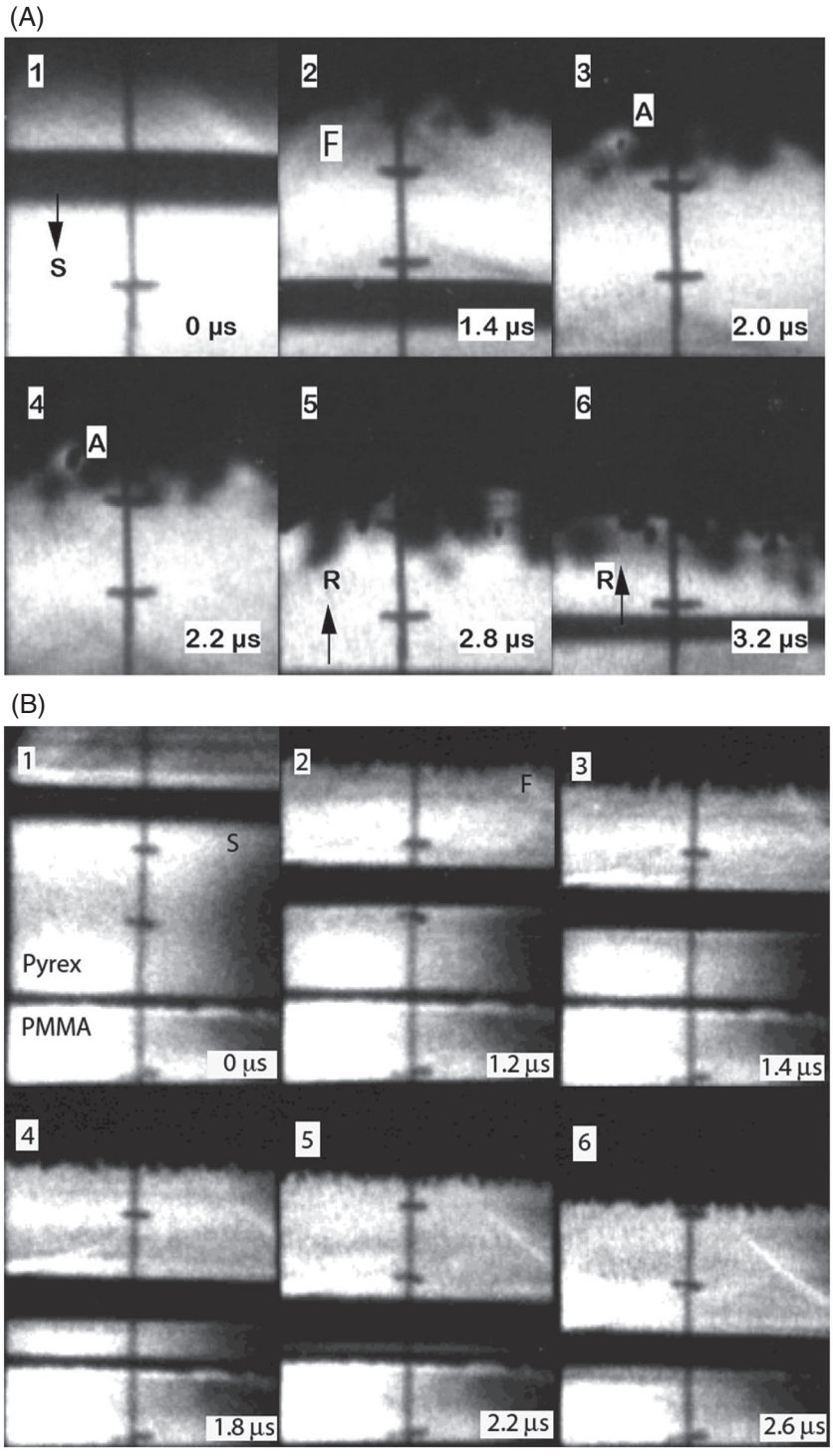

Figure 12: (A) Soda-lime glass impacted from the top at 250 m s^{-1}. (b) Borosilicate (Pyrex) glass impacted from the tops at 250 m s^{-1}. In both cases, a shock S and a failure front F travel down through the frames. The scale markers are 5 mm apart, and the first is 15 mm from the impact face. For the soda-lime case, a damage site, A, nucleates and grows ahead of the failure front in frames 3 and 4. The reflected release R from the free surface enters the frame from below in frames 5 and 6. For the borosilicate case, the white line entering from the right in frame 4 is believed to be lateral release. From [130]

trajectories form a cone for a fully developed elastic stress field [181–183], the details of which were worked out qualitatively by Heinrich Hertz [184–186] (see Figure 20A) and subsequently more accurately by Huber [187] and Fuchs [188] (see Figure 20B). For a discussion of these matters, see [189].

© 2013 Wiley Publishing Ltd
doi: 10.1111/str.12075

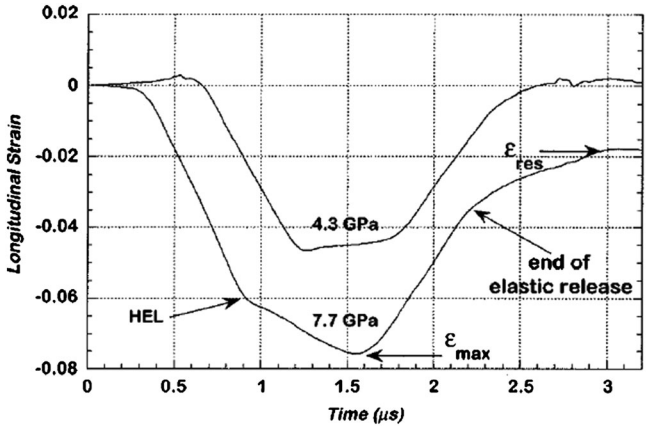

Figure 13: Strain gauge records from soda-lime glass shocked below and above the Hugoniot elastic limit (HEL). From [149]

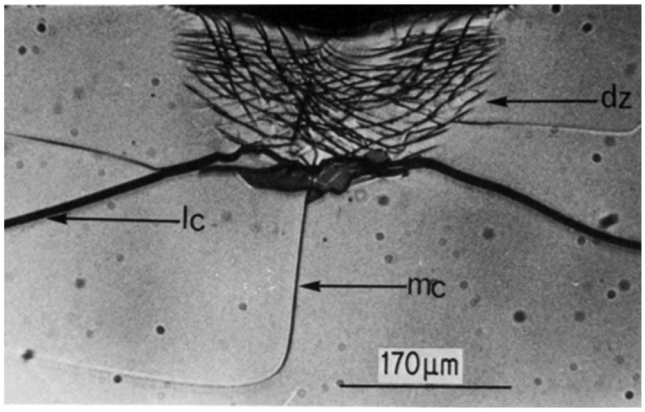

Figure 14: Damage beneath a Vickers indentation in soda-lime glass loaded to 100 N. 'dz' indicates deformed zone, and 'mc' and 'lc' indicate median crack and lateral crack, respectively. From [154]

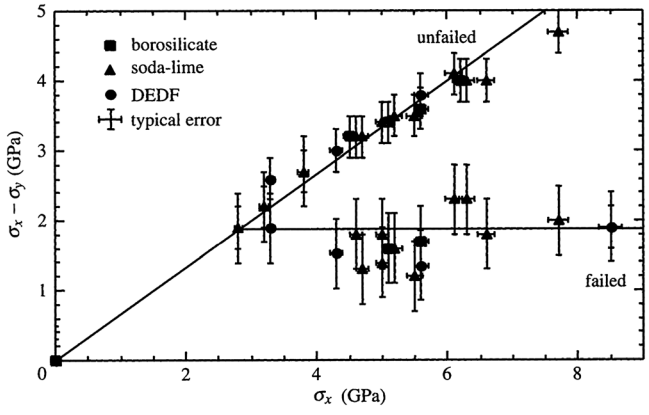

Figure 15: Variation of the shock shear strength of three different silica-based glasses in the failed and unfailed states. From [114]

Stimulated by Hertz's and Huber's analyses, there have been a number of high-speed photographic studies of the development of cone crack (and other crack systems)

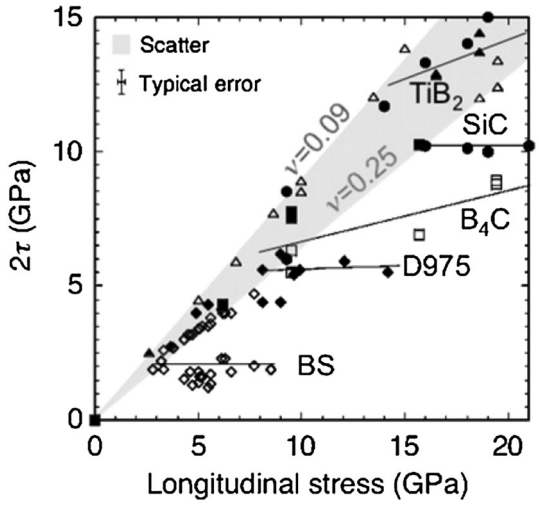

Figure 16: Plot of the deviatoric response 2mm from the impact face for a number of armour ceramics and a borosilicate (BS) glass. D975 is an alumina. The grey shaded region is enclosed bounded by lines for a material with Poisson ratio 0.09 (TiB2) and 0.25 (glasses). From [167]

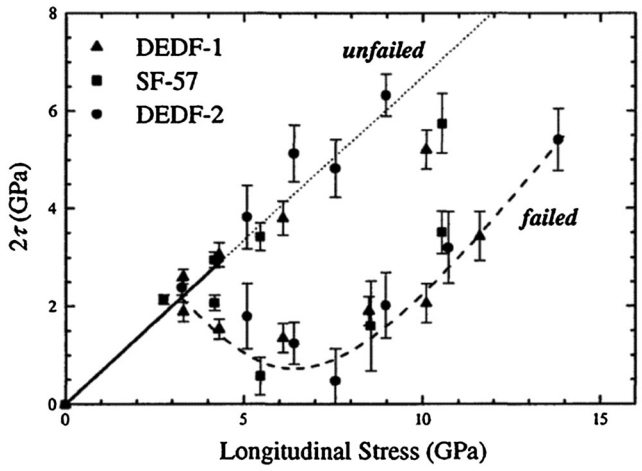

Figure 17: Deviatoric responses of dense glasses tested up to ca.14 GPa longitudinal stress. From [168]

in glass caused by solid particle impact; see, for example, [77, 190–199]. Note that the angle of the cone depends on both the speed and angle of impact [190, 195, 200, 201]. On the impact surface itself, the crack pattern forms a ring (Figure 21). The diameter of the ring crack is close to, but not identical with, the maximum diameter of the flat formed on the impacting sphere during impact. The reasons why the two diameters are not the same include (i) friction affecting the position of maximum stress on the surface [202] and (ii) the size and position distributions of surface cracks [203–208] (see also Figure 22).

The connection of these cone-crack ideas to ceramic-faced body armours was made by Field and co-workers [209, 210]; see also Figures 23 and 24. Basically, the formation of a cone helps protect a person wearing the armour from harm in two

© 2013 Wiley Publishing Ltd
doi: 10.1111/str.12075

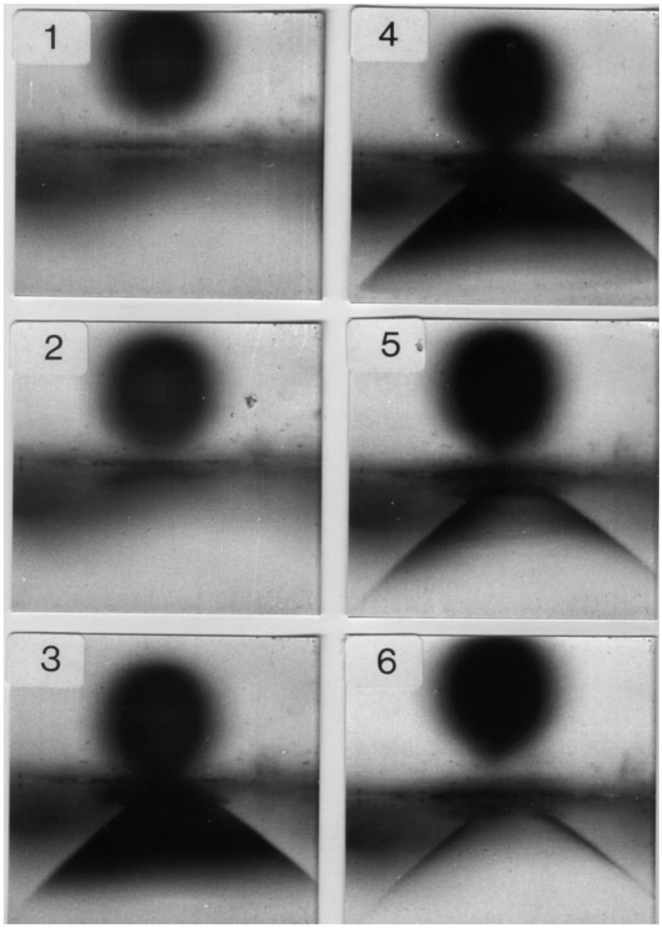

Figure 18: High-speed photographic sequence (1 μs interframe time) of the impact of a 1-mm-diameter glass sphere on borosilicate glass at 125 m s^{-1}. From [190]. The darkening and lightening of the crack are due to its opening and closing. The ball is out of focus because the camera was focussed on the cone crack, and the depth of field of the lens used was small (the glass block was 25 mm thick in the line of sight).

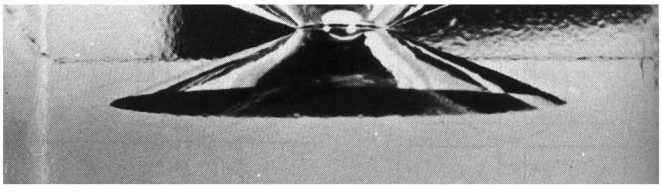

Figure 19: Cone crack produced by ball indent on soda-lime glass. From [172]

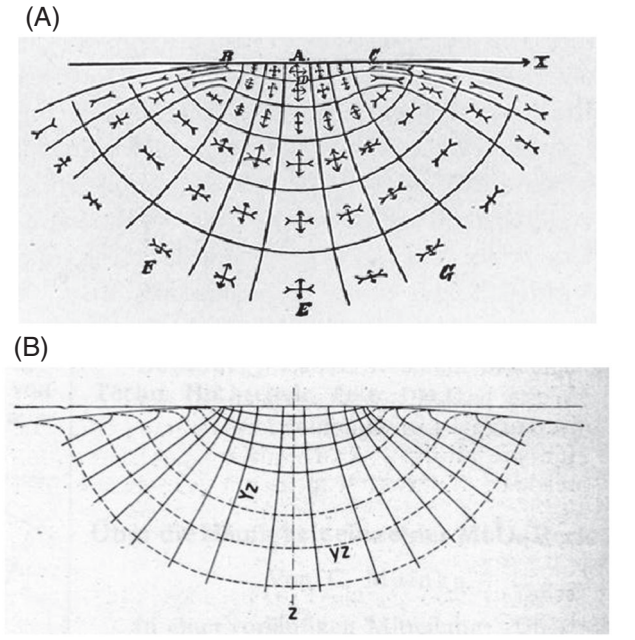

Figure 20: (A) Hertz's schematic (qualitative) diagram of the principal stresses produced by loading an elastic flat by an elastic sphere. From [186]. (B) More accurate representation of the principal stresses beneath an elastic sphere on a flat indentation as calculated by Fuchs [188]

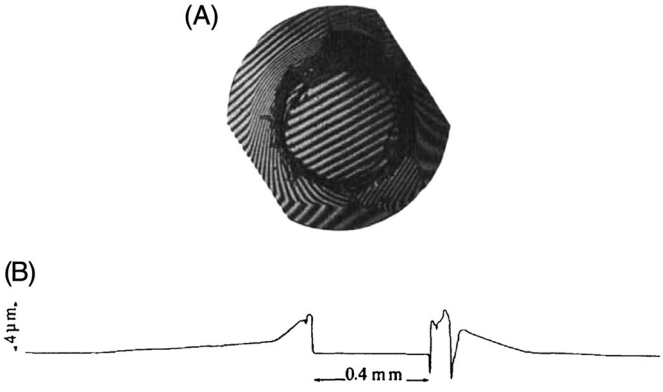

Figure 21: (A) Interferogram of the damage to a block of soda-lime glass produced by the normal impact of a 1-mm-diameter glass sphere at 120 m s^{-1}. (B) Talysurf trace across the same impact site. Note that the region inside the ring crack is flat, while that outside has risen above the original level of the surface. From [190]

ways: (i) the fragment ejected from the rear of the tile travels much more slowly than the bullet, and (ii) the area over which the load is applied by the cone-shaped fragment is much larger than that of the bullet. Note from Figure 23 that alumina is better than glass in body armour applications because (a) it spreads the load over a larger area and (b) it produces a cone at velocities an order of magnitude greater than those of glass. If the tile is backed up by a tough viscoelastic composite (e.g. Kevlar), the effect of the fragment can be cushioned even more: the person will be bruised but not penetrated by the impact. Note that this mechanism only applies up to impact speeds that are some critical fraction of the elastic wave speed in the ceramic (or glass) because in order to form a cone, a 'quasistatic' elastic stress field has to have time to be established (see, for example, Figure 1). It has also been observed that the nature of the backing material can have an effect on the cone [198].

© 2013 Wiley Publishing Ltd
doi: 10.1111/str.12075

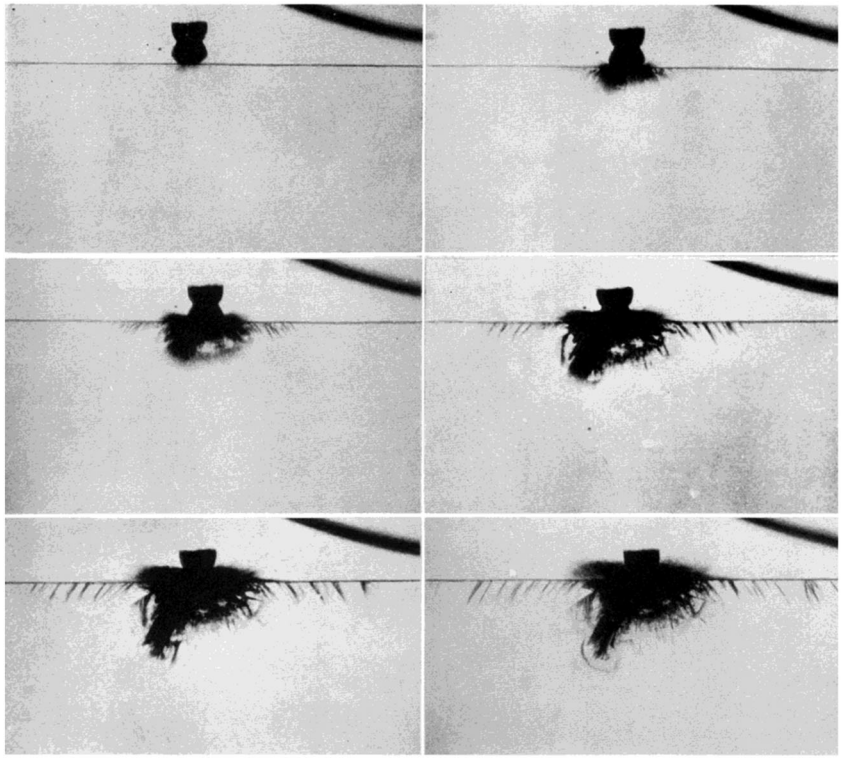

Figure 22: High-speed photographic sequence of the impact of a lead slug on the edge of a $76 \times 76 \times 3.1$-mm sheet of glass at $210\,\mathrm{m\,s^{-1}}$. Interframe time 1.94 μs. The point on the surface at which fresh cracks appear moves outwards at the Rayleigh wave velocity ($3100\,\mathrm{m\,s^{-1}}$). From [206]

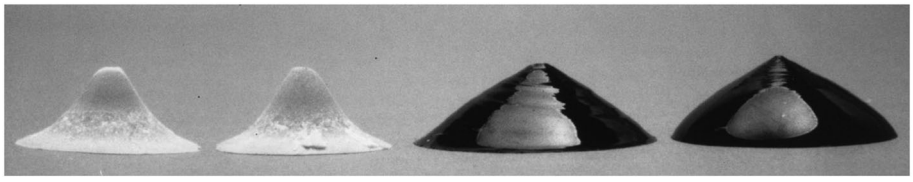

Figure 23: Cones ejected from the rear of alumina (white, left) and glass (dark, right). Note that the stress wave interaction has caused the alumina cones to broaden at their base (and hence spread the load over a wider area) but narrow in the case of the glass (this phenomenon can be seen developing in Figure 24). The impacts were performed with 5-mm-diameter steel spheres. The alumina targets were impacted at 302 and $356\,\mathrm{m\,s^{-1}}$. The glass targets were impacted at $35\,\mathrm{m\,s^{-1}}$. From [209]

As silica-glass windows are required to be transparent, fibrous composite materials cannot be used as a backing. However, in the 1940s, tough transparent polymers became available, and these were put into service to form glass/polymer laminates [34, 211]. The use of such structures where bullet resistance is required (e.g. in vehicles) is more recent [43, 45, 212–214]. A typical laminate structure consists of a hard silica-glass front face bonded to and backed by a polycarbonate back face (more complex laminated structures may be used depending on the expected threat). The intermediate bonding layer also has to be transparent and is usually either polyvinyl butyral or a polyurethane. The laminate works by the glass front face first blunting the bullet and slowing it down sufficiently that the polymer back face can capture and stop it. Problems arise over time due to embrittlement of the polycarbonate due to physical and chemical ageing [215–220]. Elastic wave reverberation within the laminate layers may also intensify the stresses at certain well-defined radii [221] (Figure 25), leading to spalling of the polycarbonate as the temperature is lowered [45] (Figure 26). Thus, below a certain critical temperature, a glass-fronted laminated bullet-proof window may become useless even when new. A review of the frequency response of laminated glass has recently been published [222].

Debris picked up by strong winds (e.g. hurricanes and tornados) has a relatively low impact speed (*ca.* $40\,\mathrm{m\,s^{-1}}$)

© 2013 Wiley Publishing Ltd
doi: 10.1111/str.12075

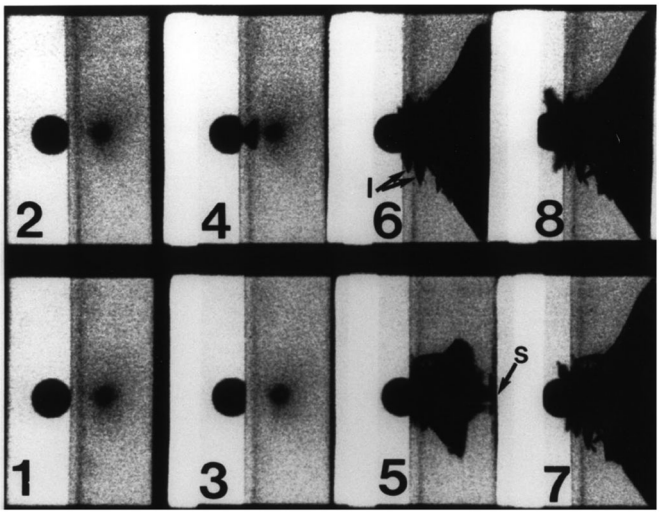

Figure 24: High-speed photographic sequence of the impact of a 5-mm-diameter steel sphere onto a 10-mm-thick soda-lime specimen at 92.5 m s^{-1}. From [209]

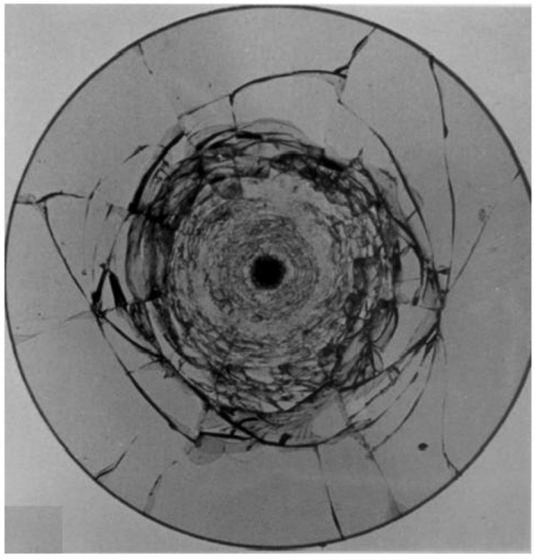

Figure 25: Photograph of 152-mm-diameter laminate disc after impact with a 6-mm-diameter steel ball at 350 m s^{-1} at a temperature of −28.5 °C. From [45]

compared to bullets. However, the impactors can be large (kg masses) and made of materials such as wood whose dynamic properties are not as well studied or understood as other materials [5, 223–239], making the phenomenon harder to model and analyse than classic ballistic impact (Figure 27).

There are very few papers about single high-speed water drop impact on silica glasses [206, 221, 240–242], despite the fact that impact on water drops on glass at 100–1000 m s^{-1} (typical of aircraft speeds) can produce significant damage (Figures 28 and 29). Most such studies have been performed on infrared-transparent radome materials for missiles and military aircraft (e.g. [243–247]).

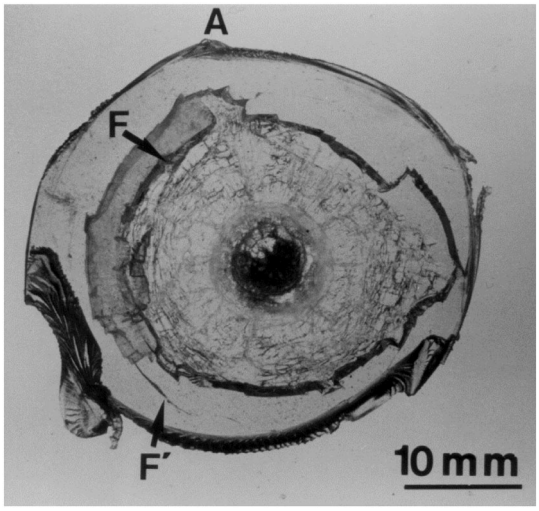

Figure 26: Photograph of a typical spall fragment. Note that the radius of the interlayer is smaller than that of the polycarbonate. The fractured glass has imprinted and cut the interlayer material. There are several fractures under the interlayer material at, for example, F and F′. These fractures are associated with fracture bands in the glass. The outer boundary is made up of several segments due to cracks initiating at more than one site. 'A' marks the boundary between two cracks. From [45]

Figure 27: Crack pattern produced in a laminated window impacted by a wooden block at 15 m s^{-1}. From [5]

There are both similarities and differences between the impact sites produced by solid particle (Figure 30) and liquid drop impact (Figure 31A). Both types of impact typically produce an apparently damage-free central and circular region surrounded by a ring of intense fracture. Solid particle impact can produce a cone crack (Figures 18, 24, 30, and 32), which to my knowledge has never been seen under liquid impact, probably because the shock is applied for so short a time that the stress field does not develop into the quasistatic or Hertzian form.

Additional crack systems (termed 'median' and 'lateral') can also form during solid impact (Figures 32 and 33), and if the impact velocity is high enough, these can obscure the

© 2013 Wiley Publishing Ltd
doi: 10.1111/str.12075

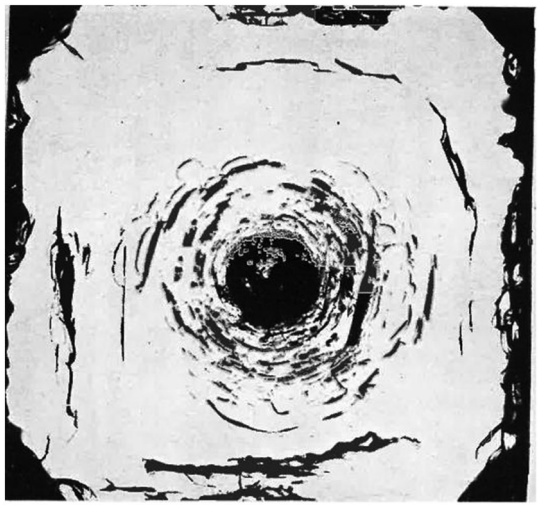

Figure 28: Damage produced to a 25.5-mm (1-in.) glass cube by the high-speed impact of a single water drop at *ca.* 1000 m s^{-1}. Note the spall damage produced by stress wave reflection at the corners and sides. From [240]

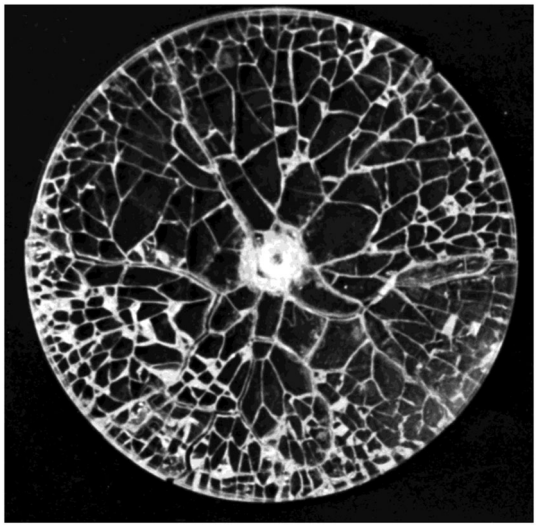

Figure 29: Photograph of a 50-mm-diameter, 3-mm-thick disc of thermally toughened glass shattered by the impact of a drop of water at 700 m s^{-1}. From [242]

contact zone [190, 191]. Plastic deformation may occur in glass due to solid particle impact if the contact zone is small enough (Figure 33). So for any given particle size, there will be a transition from plastic to brittle behaviour as the impact velocity is increased (see Figure 34). Slikkerveer and co-workers [248] found this behaviour for both soda-lime and borosilicate glasses despite them having very different network structures on the atomic scale. Quasistatic indentation studies of plasticity in glass have been performed by a number of researchers over many years, e.g. [154, 176, 249–270].

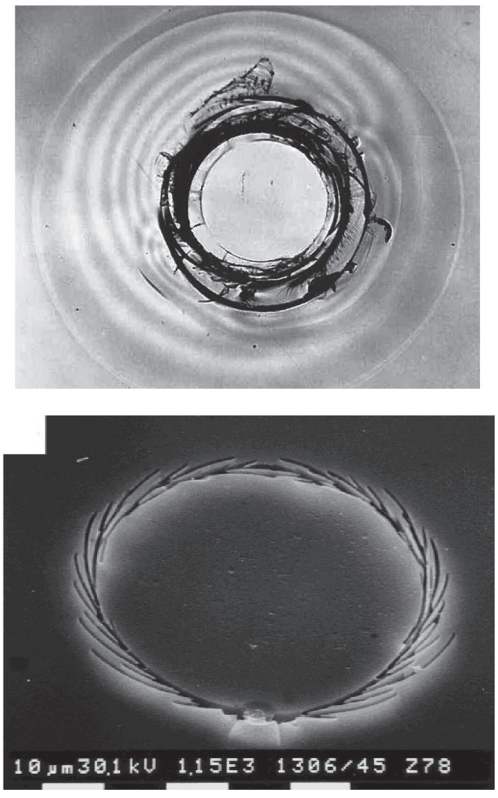

(a)

(b)

Figure 30: (A) Optical photograph of damage site produced in plate glass by the impact of a 12.7-mm-diameter steel ball at 5 m s^{-1}. From [221]. (B) Scanning electron micrograph of a damage site produced by a single impact of an approximately 180-µm-sized spherical ceramic sphere (exact impact velocity not known) on a borosilicate glass (AF45). From [248]

Another major difference between liquid and solid impacts is that a water drop flows rapidly across the surface after the initial shock compression has been released [206, 221, 240]. This jetting extends the cracks opened up outside the ring crack by the passage of a short-duration Rayleigh wave (Figures 22 and 31). The damage to a glass disc can be assessed by applying a uniform pressure to the back surface (burst test) [271]. Additional water drop impacts at the same site sharpen the residual strength/velocity curve but do not displace its position (Figure 35).

Studies where glass was subjected to long-term multiple-solid-particle impact showed that unlike ductile materials where many impacts have to take place near a particular place before enough damage occurs for material removal [273], mass loss occurs in glass from the very beginning (see Figures 36 and 37) [248, 274–283]. There is also evidence that the rate at which material is removed *decreases* with time for silica glasses [274]. Small abrasive grits delivered to a surface in a continuous high-pressure water jet can be used to machine materials including silica glasses (e.g. [284–288]).

© 2013 Wiley Publishing Ltd
doi: 10.1111/str.12075

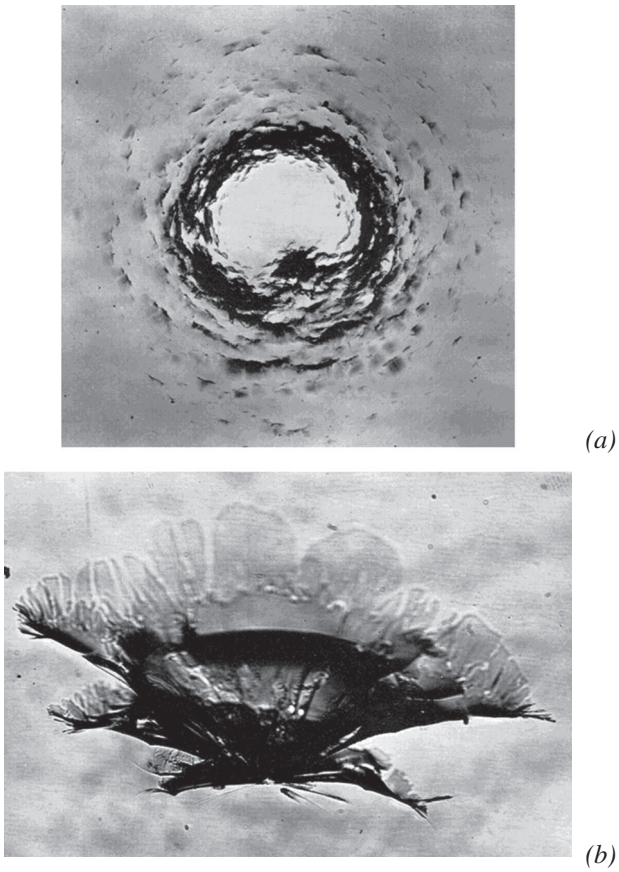

Figure 31: (A) Damage produced on the surface of plate glass by the impact of a 3-mm-diameter drop of water at 650 m s^{-1}. (B) High-magnification photograph of one of the circumferential cracks. From [221]

4. Hypervelocity Impact

The fastest impacts on man-made objects take place not on the battlefield but on spacecraft due either to micrometeoroids or orbiting space junk (although shaped charges can approach these velocities). Manned spacecraft, such as the former Space Shuttle, require transparent windows. Hence, a number of studies have been performed on the hypervelocity impact properties of glass, e.g. [291–308]. This research is relevant even to unmanned spacecraft as they often have external glass-coated or glass-shielded components (e.g. [300, 309–313]).

The morphology of hypervelocity impact sites on glass was studied by Mandeville and Vedder [291, 314]. As they used an electrostatic method of acceleration, the highest velocities were only achievable using small particles. This explains why in Figure 38 the crater size increases up to frame C but decreases thereafter. However, their studies allowed changes in morphology of craters to be determined as a function of velocity for polystyrene impactors. As polystyrene has a low density, the glass surface simply dents up to about 3 km s^{-1}. But between about 3 and 5 km s^{-1}, a lip reminiscent of a frozen splash formed around the crater. Above this velocity, cracks appeared around the hole. The velocity thresholds for these changes in behaviour are lower for higher-density projectiles [315]. The effect of the specimen boundaries on the damage imparted to a glass target by hypervelocity impact has been highlighted by Yang and co-workers [305].

Turning the tables somewhat, glass has also been used since the Second World War as a shaped charge material for demolition purposes [316] and in what are now called 'improvised explosive devices' [317]. Beer and wine bottles have sometimes been used because their bases often have a conical indent (Figure 39) [318]. Glass has also been experimented with as a shaped charge material for fracturing rock down oil wells, but its penetration depth was found not to be adequate [316]. Depending on the density of glass used, the jet formed is either highly particulated or amongst the most ductile known (Figure 40) [318]. Under certain circumstances, a glass shaped charge jet can even be hollow. For recent discussions of glass shaped charges, see the papers by Baker *et al*. [318], Cowan & Bourne [319], and Edwards *et al*. [320]. None of these authors discuss the mechanisms through which glass shaped charge jets form.

5. Constitutive Modelling

In order to be able to model glass in ballistic applications, it is necessary to have a constitutive model for it, i.e. we need to know the stress a particular glass can support as a function of hydrostatic pressure, strain, strain rate, and temperature in both its damaged and undamaged states. We also need to know how a glass makes the transition to a damaged state, i.e. the kinetics of the process [321–324] (see also Figure 41). These matters are being actively investigated [324–332].

The main dynamic brittle fragmentation models in the literature are those due to Mott [334–338], Grady and Kipp [333, 339–346] and Johnson and Holmquist [324, 347–349]. Mott originally developed his model during the Second World War for the explosive fragmentation of shell cases. Grady and Kipp also had this problem in mind when they developed their model, but they also applied it to a variety of problems including fracture of oil shales [350], rocks in general [351], armour ceramics [352] and glass [342].

A feature of the Grady–Kipp model relevant to shock loading and subsequent failure of brittle materials such as glass is the postulate of the existence of a dynamic failure surface lying *above* that determined quasistatically (Figure 41). The position of this upper surface is independent of the position of the lower (quasistatic) surface. An implicit assumption they make is that the position of the HEL of brittle materials is a manifestation of fracture kinetics. Hence, it should be strain rate dependent. Evidence for this has been presented in terms

© 2013 Wiley Publishing Ltd
doi: 10.1111/str.12075

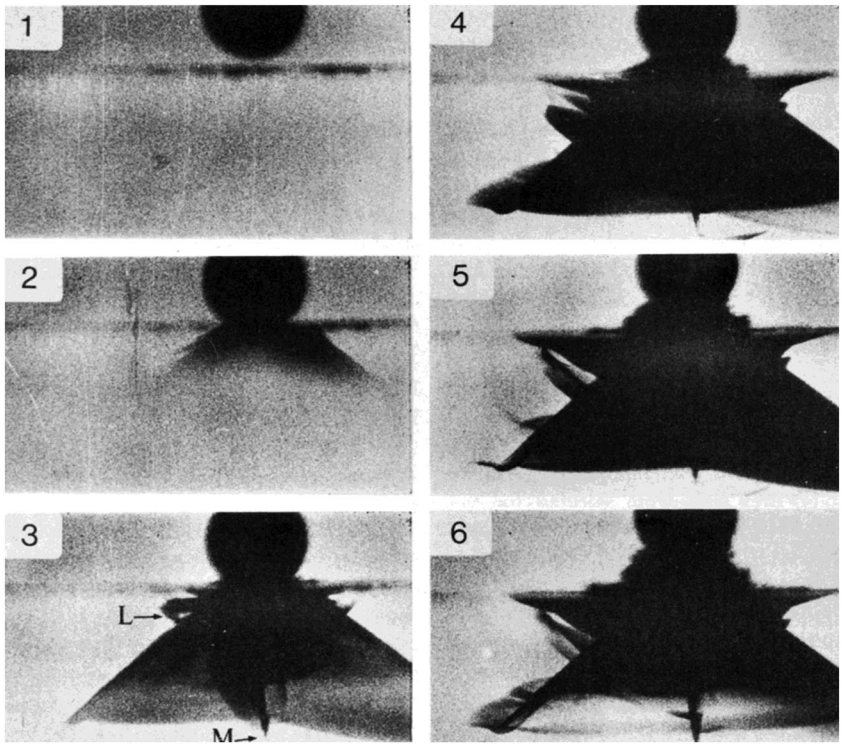

Figure 32: High-speed photographic sequence of the impact of a 1.0-mm-diameter steel ball on Pyrex (borosilicate) glass at 200 m s^{-1}. Interframe time 1 μs. In frame 3, L indicates lateral crack, and M indicates median crack. From [191]

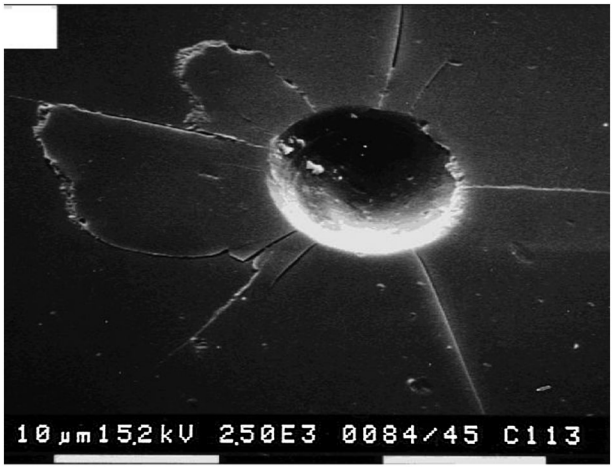

Figure 33: Scanning electron micrograph of a damage site produced by a single impact of an approximately 180 μm-sized spherical ceramic sphere (exact impact velocity not known). Note that the diameter of the contact zone is smaller than for the impact shown in Figure 30b. From [248]

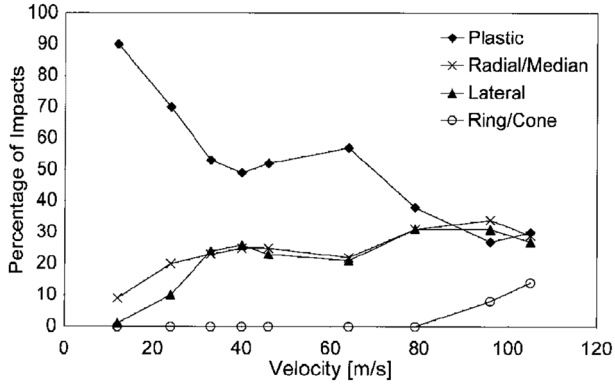

Figure 34: Graph showing the fraction of impacts that produced plastic as opposed to brittle behaviour for impacts of approximately 180 μm-sized ceramic particles on a borosilicate glass as a function of impact velocity. From [248]

of elastic precursor decay for various ceramics, e.g. [353–356], although doubts have been expressed about this interpretation of the data [163]. Anyway, Grady has said [338, 341] that in some circumstances, the older model of Mott [336] is superior to his own.

Chocron and co-workers have performed a quasistatic study of the effect of confining pressure on the strength of damaged and undamaged borosilicate and soda-lime glasses with the aim of providing constitutive data for numerical modelling of ballistic impact on glass [325–328,332]. They used two different methods of applying pressure and axial loads (Figure 42). They interpreted their data in terms of two stress-dependent soil mechanics models (see Figure 43):

© 2013 Wiley Publishing Ltd
doi: 10.1111/str.12075

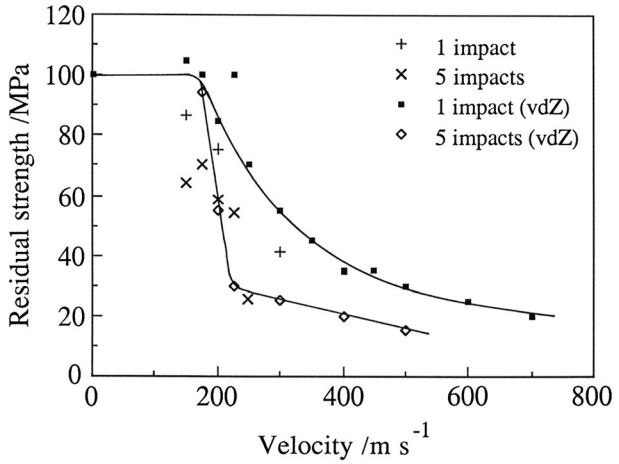

Figure 35: Residual strength versus water drop impact velocity for soda-lime glass. The two curves present data where either one or five impacts were performed on the same site in the middle of the disc. From [242]. Some of these data had previously been presented in [272]

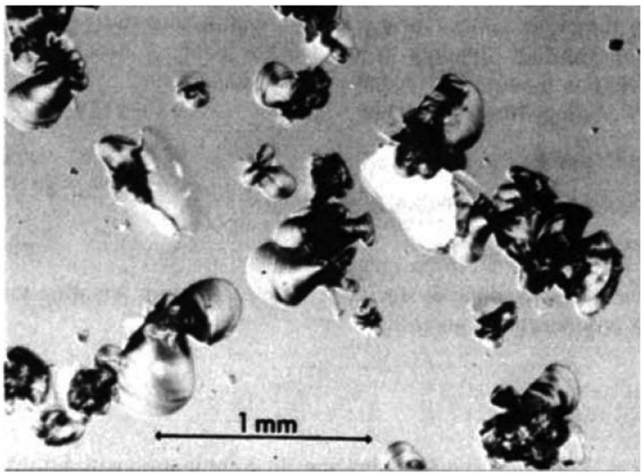

Figure 36: Optical micrograph of soda-lime glass surface after normal impact by 100-mesh SiC particles at 113 m s^{-1}. From [289]

(i) the Drucker–Prager [357] (see Equation (1)) and (ii) the Mohr–Coulomb [358] (see Equation (2)):

$$Y = \begin{cases} Y_0 + \beta P & P < (Y_{\text{cap}} - Y_0)/\beta \\ Y_{\text{cap}} & P \geq (Y_{\text{cap}} - Y0)/\beta \end{cases} \quad (1)$$

where Y_0 is the strength at zero pressure, P is the hydrostatic pressure (taken as the negative of the mean stress), β is the slope of a plot of Y versus P and Y_{cap} is the limiting flow stress;

$$\tau = c + \mu\tilde{\sigma}_n \quad (2)$$

where c is the cohesion, μ is the friction coefficient and $\tilde{\sigma}_n$ is the normal stress (taken as positive in compression). They also compared their data to those obtained dynamically under shock conditions (Figure 44).

Their main conclusions were as follows: (i) the pressure dependence (Drucker–Prager) and the friction coefficient (Mohr–Coulomb) are independent of damage; (ii) the zero-pressure strength (Drucker–Prager) or cohesion (Mohr–Coulomb) decreases with increasing damage; and (iii) the strength of comminuted glass does not depend on strain rate.

The recently published Holmquist–Johnson model for glass [324] is presented graphically in Figure 45. The graphs show how three parameters vary as a function of pressure (absolute values are not given): (a) strength, (b) failure strain, and (c) density. Note that their model takes account of the differences in the strength of glass at the surface, within the bulk and close to failed material (Figures 45A and 46). Despite its complexity, they found that using it did not match the experiment over the whole velocity range for a series of ballistic experiments. They have since extended the comparison to the hypervelocity case [307].

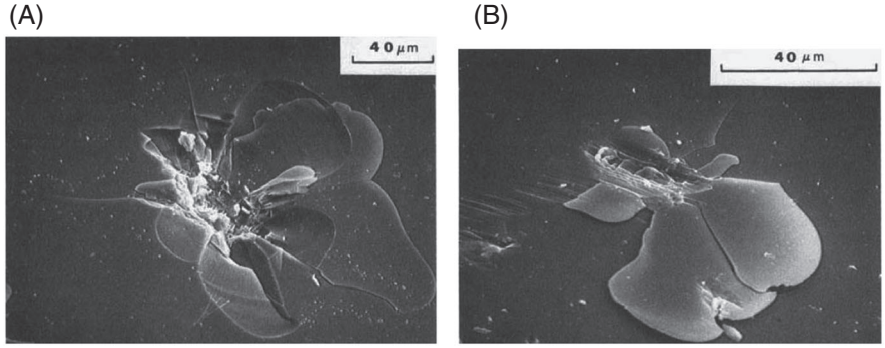

Figure 37: Scanning electron micrographs of damage sites produced on crown glass by (A) the normal impact and (B) the oblique impact (15°) of 100-mesh SiC particles at 94 m s^{-1}. From [290]

© 2013 Wiley Publishing Ltd
doi: 10.1111/str.12075

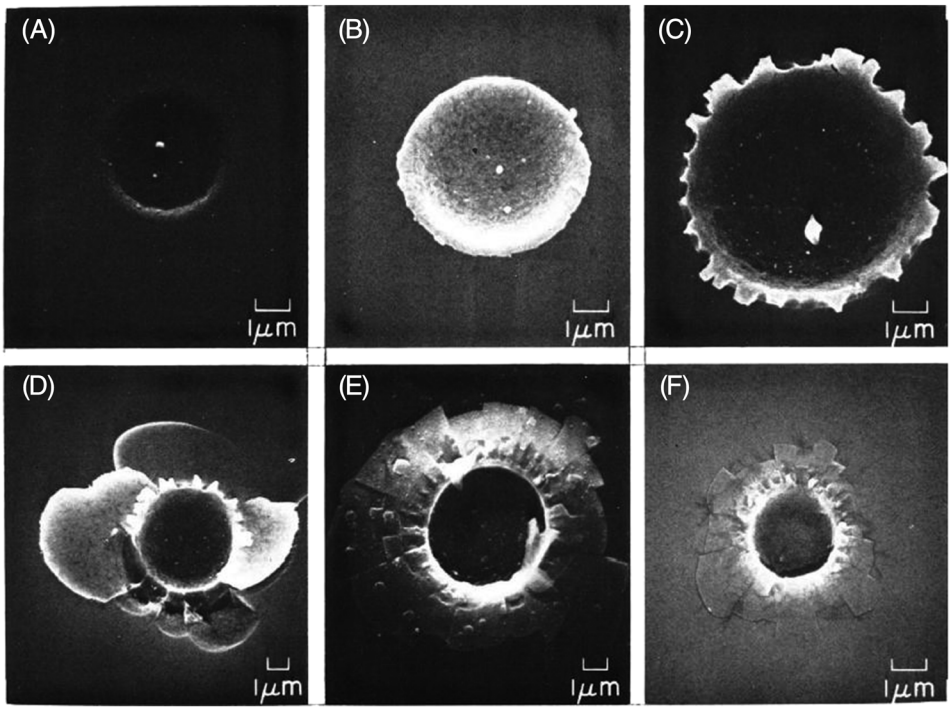

Figure 38: Scanning electron micrographs of impact sites on soda-lime glass produced by the normal hypervelocity impact of polystyrene spheres of varying masses m. (A) $m = 42.2$ pg, $v = 2.95$ km s^{-1}; (B) $m = 28.6$ pg, $v = 4.15$ km s^{-1}; (C) $m = 57.7$ pg, $v = 5.05$ km s^{-1}; (D) $m = 27.5$ pg, $v = 5.38$ km s^{-1}; (E) $m = 17.0$ pg, $v = 8.22$ km s^{-1}; (F) $m = 1.67$ pg, $v = 12.6$ km s^{-1}. From [314]

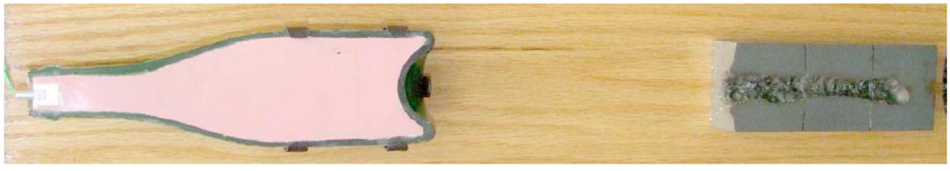

Figure 39: Cross section of a beer bottle filled with Octol 70/30 explosive (left) and resulting penetration of steel from a similar shaped charge (right). From [318]

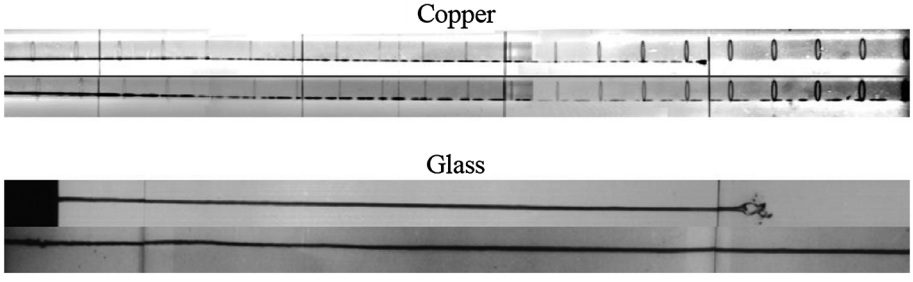

Figure 40: Flash X-ray images of copper and glass shaped charges at a standoff of 20 charge diameters. From [318]

© 2013 Wiley Publishing Ltd
doi: 10.1111/str.12075

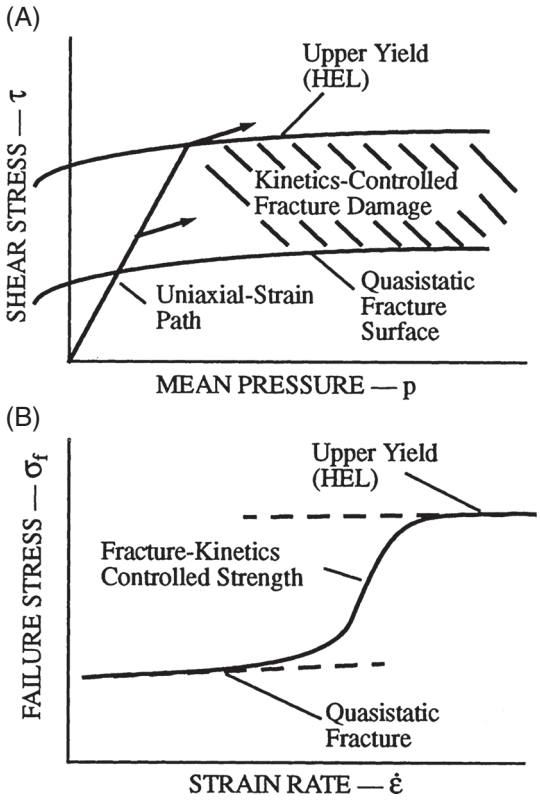

Figure 41: (A) Schematic diagram of the Grady–Kipp model applied to shock loading and failure of brittle materials. (B) Consequences for kinetics of failure and position of the Hugoniot elastic limit (HEL). From [321, 333]

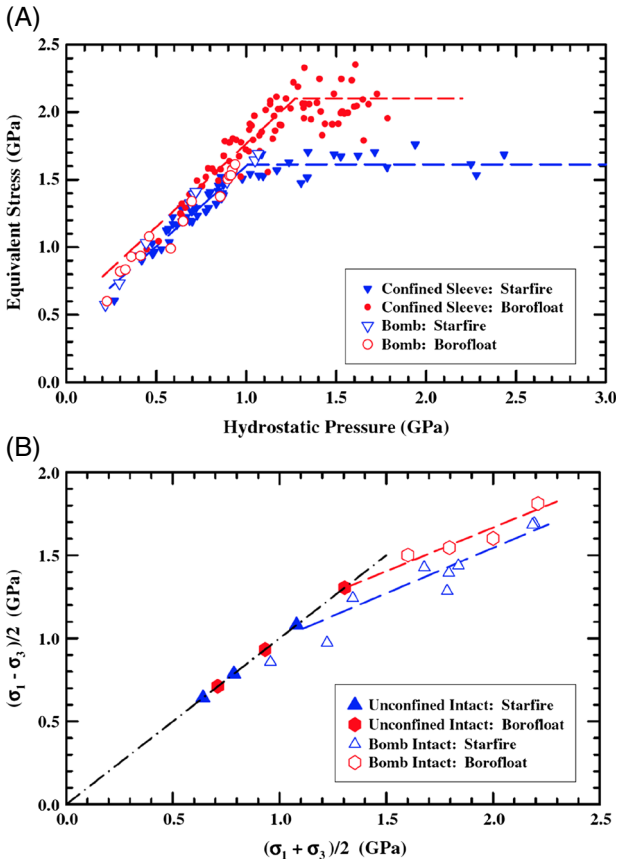

Figure 43: (A) Fit of glass data to Drucker–Prager constitutive model. (B) Fit of glass data to Mohr–Coulomb constitutive model. 'Starfire' is a soda lime and 'Borofloat' a borosilicate glass. From [327]

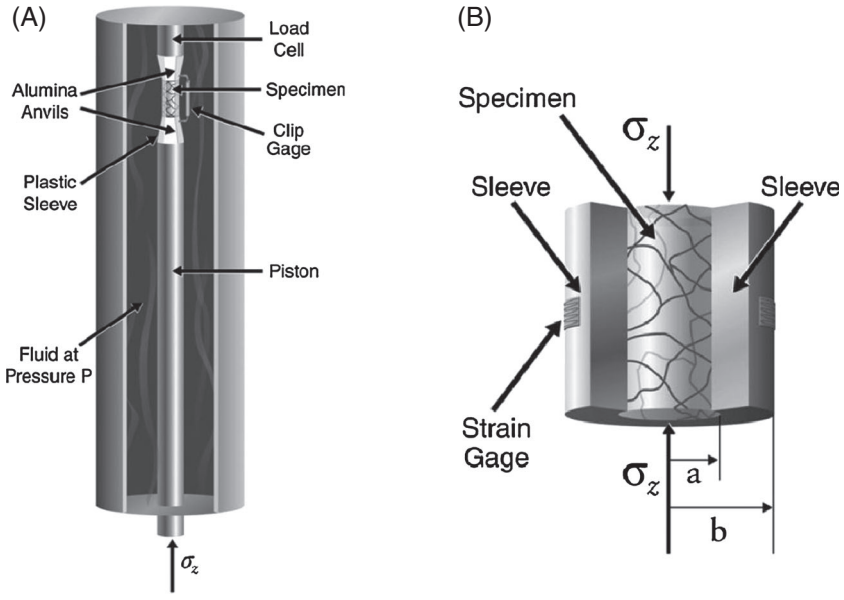

Figure 42: (A) Schematic diagram of hydraulic bomb used for loading glass specimens. (B) Confined sleeve technique for loading damaged glass specimens. From [327]

© 2013 Wiley Publishing Ltd | *Strain* (2014) **50**, 470–500
doi: 10.1111/str.12075

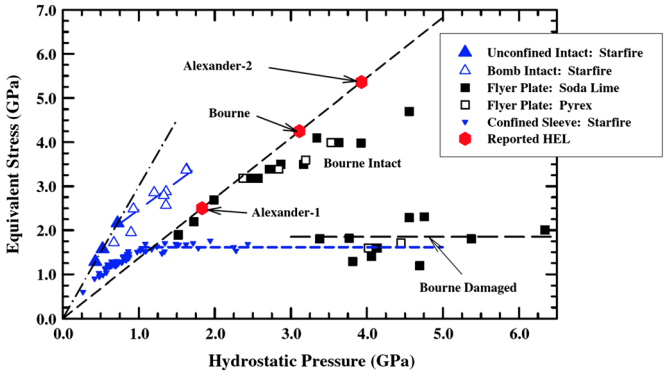

Figure 44: Comparison of hydrostatic data with plate impact results. From [327]. HEL, Hugoniot elastic limit

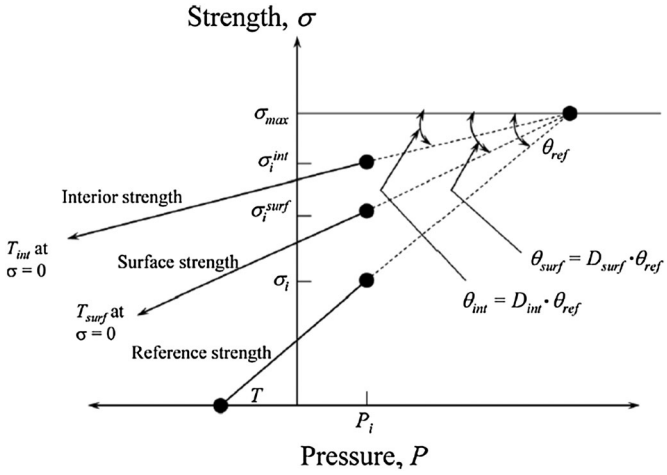

Figure 46: Graphical description of the interior, surface, and reference strength for the Holmquist–Johnson strength model. From [324]

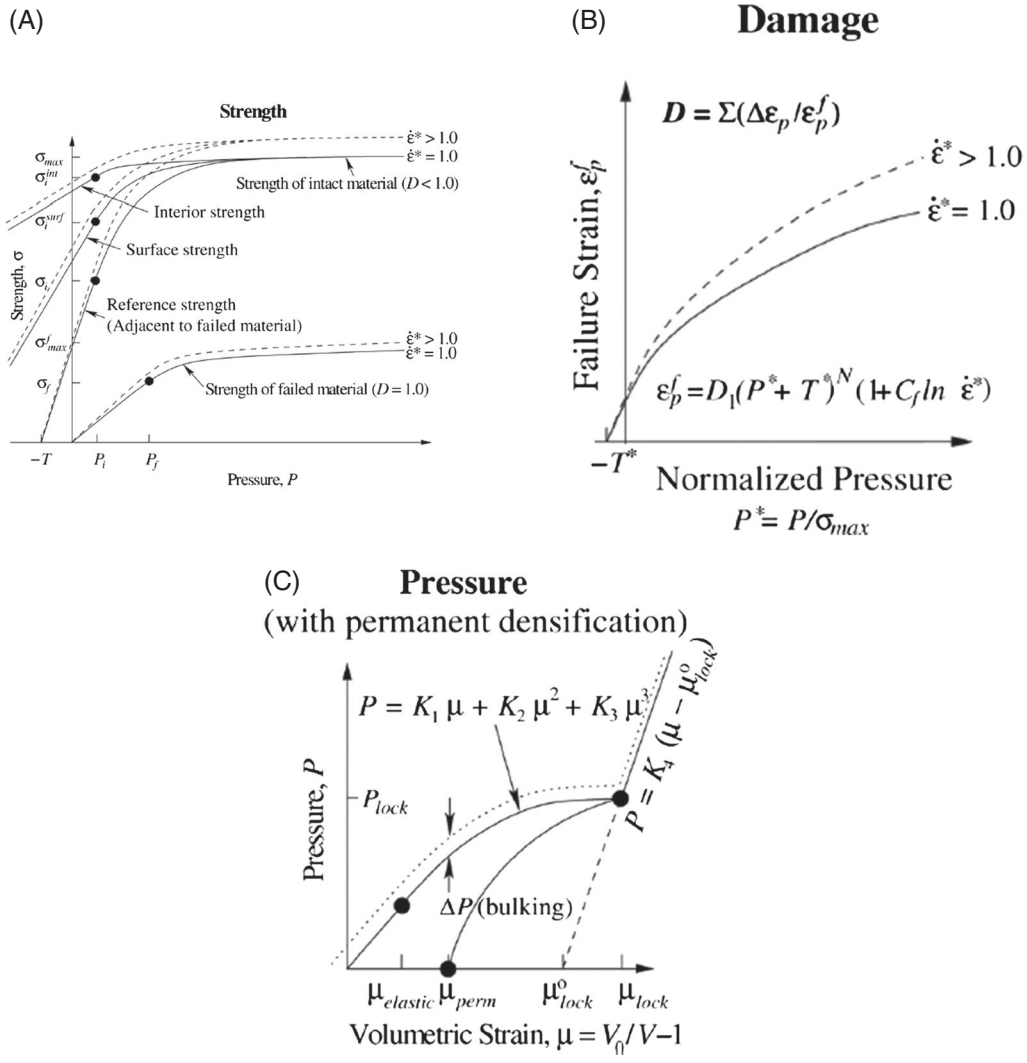

Figure 45: Graphical presentation of Holmquist–Johnson constitutive model for glass. From [324]

© 2013 Wiley Publishing Ltd |
doi: 10.1111/str.12075

6. Summary

Optical transparency is often required alongside resistance to impact. At present, silica glasses remain one of the few materials able to deliver this, despite their brittleness. The intention of this introductory review was to give a way in to the literature on the properties of glasses under impact, the methods of study, and the present state of constitutive modelling. The two types of glass that have been most studied are soda lime and borosilicate. Some differences between the behaviours of these two types have been reported, but the origin of these differences has not been conclusively demonstrated.

In the future, densification due to collapse of the atomic structure needs to be clearly distinguished from compaction of comminuted material. Insights from research on granular materials need to be brought to bear on this problem, recognising that until substantial flow occurs, the behaviour of comminuted glass will be different to, say, sand. I would suggest that the way forward will be to bring in insights from polymer physics (e.g. the Porter–Gould model [359, 360]), fracture [324, 331] and granular mechanics [361, 362]. Observed differences between glass and metallic shaped charge jets probably lie in what happens as they are formed. Understanding the differences will require a combination of experiment and modelling.

ACKNOWLEDGEMENTS

I would like to thank Prof. F. Bobaru, Dr M. M. Chaudhri, Dr I. G. Cullis, Prof. J. E. Field and Dr P. J. Gould for comments on this review.

REFERENCES

1. Beason, W. L., Meyers, G. E. and Reason, R. W. (1984) Hurricane related window glass damage in Houston. *ASCE J. Struct. Engng* **110**, 2843–2857.
2. Behr, R. A. and Kremer, P. A. (1996) Performance of laminated glass units under simulated windborne debris impacts. *ASCE J. Architectural Engng* **2**, 95–99.
3. Bole, S. A. (1999) Investigation of the mechanics of windborne missile impact on window glass. MS thesis, Texas Tech., Lubbock, TX.
4. Masters, F. J., Gurley, K. R., Shah, N. and Fernandez, G. (2010) The vulnerability of residential window glass to lightweight windborne debris. *Engng Struct.* **32**, 911–921.
5. Zhang, X., Hao, H. and Ma, G. (2013) Laboratory test and numerical simulation of laminated glass window vulnerability to debris impact. *Int. J. Impact Engng* **55**, 49–62.
6. Pugh, E. M., Heine-Geldern, R.v., Foner, S. and Mutschler, E. C. (1952) Glass cracking caused by high explosives. *J. Appl. Phys.* **23**, 48–53.
7. Harris, R. J., Marshall, M. R. and Moppett, D. J. (1977) The response of glass windows to explosion pressures. *Inst. Chem. Engrs Symp. Ser.* **49**, 83–97.
8. Makovicka, D. and Lexa, P. (1992) Dynamic response of window glass plates under explosion overpressure. In: P. S. Bulson (ed) Structures under Shock and Impact II. Computational Mechanics Publications, Southampton: 381–392.
9. Makovicka, D. (1998) Shock wave load of window glass plate structure and hypothesis of its failure. In: N. Jones, D. G. Talaslidis, C. A. Brebbia and G. D. Manolis (eds) Structures under Shock and Impact V. Computational Mechanics Publications, Southampton, UK: 43–52.
10. Dharani, L. R., Wei, J. and Ji, F. S. (2002) Failure analysis of laminated architectural glass panels subjected to blast loading. In: N. Jones, C. A. Brebbia and A. M. Rajendran (eds) Structures under Shock and Impact VII. WIT Press, Southampton, UK: 37–46.
11. Dharani, L. R. and Wei, J. (2004) Dynamic response of laminated glass under blast loading: effect of negative phase. In: N. Jones and C. A. Brebbia (eds) Structures under Shock and Impact VIII. WIT Press, Southampton, UK: 181–190.
12. Marchand, K. A., Conrath, E. J., Stevens, D. J. and Meyer, S. B. (2006) Blast induced glass hazards: a comparison of design approaches and recent research. In: N. Jones and C. A. Brebbia (eds) Structures under Shock and Impact IX. WIT Press, Southampton, UK: 259–268.
13. Weggel, D. C., Zapata, B. J. and Kiefer, M. J. (2007) Properties and dynamic behavior of glass curtain walls with split screw spline mullions. *ASCE J. Struct. Engng* **133**, 1415–1425.
14. Weggel, D. C. and Zapata, B. J. (2008) Laminated glass curtain walls and laminated glass lites subjected to low-level blast loading. *ASCE J. Struct. Engng* **134**, 466–477.
15. Larcher, M., Telch, M., Gebbeken, N., Solomos, G., Casadei, F., Falcon, G. A. and Samiento, S. L. (2011) Simulation of laminated glass loaded by air blast waves. *Appl. Mech. Mater.* **82**, 69–74.
16. Hooper, P. A., Sukhram, R. A. M., Blackman, B. R. K. and Dear, J. P. (2012) On the blast resistance of laminated glass. *Int. J. Solids Structures* **49**, 899–918.
17. Harper, W. W. (1939) The behavior of bullets fired through glass. *Amer. J. Police Sci.* **29**, 718–723.
18. De Kinder, J., Lory, S., Van Laere, W. and Demuynck, E. (2002) The deviation of bullets passing through window panes. *Forensic Sci. Int.* **125**, 8–11.
19. Stankiewicz, J. and White, R. L. (1971) Carbon resistors as pressure gauges. *Rev. Sci. Instrum.* **42**, 1067.
20. McJunkins, S. P. and Thornton, J. I. (1973) Glass fracture analysis: a review. *Forensic Sci.* **2**, 1–27.
21. Thornton, J. I. and Cashman, P. J. (1986) The effect of tempered glass on bullet trajectory. *J. Forensic Sci.* **31**, 743–746.
22. Preston, F. W. (1927) On shooting through glass with a rifle. *J. Soc. Glass Technol.* **11**, 283–286.
23. Finch, D. E. (1990) The shaped charge jet attack of confined and unconfined glass targets. In: Proc. 12th Int. Symp. on Ballistics. Vol. 3. American Defence Preparedness Association, Arlington, Virginia: 67–76.
24. Solvé, G. and Cagnoux, J. (1990) The behavior of Pyrex glass against a shaped-charge jet. In: S. C. Schmidt, J. N. Johnson and L. W. Davidson (eds) Shock Compression of Condensed Matter—1989. North-Holland, Amsterdam: 967–970.
25. Hauver, G. E., Netherwood, P. H., Bensk, R. F. and Melani, A. (1991) Penetration of shaped charge jets into glass and crystalline quartz. Report no. BRL-TR-3273, Ballistics Research Laboratory, Aberdeen, MD.

© 2013 Wiley Publishing Ltd
doi: 10.1111/str.12075

26. Don, R. C., Tressler, L. and Rapacki, Jr. E. J. (1992) Ballistic performance—material property relationships of glass armor versus shaped charge jets. In: Proc. 13th Int. Symp. Ballistics, Å. Persson, K. Andersson and E. B. Björck (eds). National Defence Research Establishment, Sundbyberg, Sweden: 113–122.
27. Ham, C. J. and Shrubsall, B. P. (1995) A radiographic study of the closure mechanism produced by jets penetrating glass targets. In: M. Mayseless and S. R. Bodner (eds) Proc. 15th Int. Symp. on Ballistics. Vol. 2. Technion, Jerusalem: 31–40.
28. Held, M. (1998) Glass armour and shaped charge jets. *Propell. Explos. Pyrotech.* **23**, 105–110.
29. Rumyantsev, B. V. (2008) Kinetics of cumulative jet penetration into glass. *Tech. Phys. Letts* **34**, 995–998.
30. Hazell, P. J., Lawrence, T. and Stennett, C. (2012) The defeat of shaped charge jets by explosively driven ceramic and glass plates. *Int. J. Appl. Ceram. Technol.* **9**, 382–392.
31. Moran, B., Glenn, L. A. and Kusubov, A. (1991) Jet penetration on glass. *J. Phys. IV France* **1**(C3), 147–154.
32. Kozachuk, A. A., Kozhushko, A. A., Rumyantsev, B. V., Sinani, A. B., Vlasov, A. S. and Zilberbrand, E. L. (2003) On interaction of shaped-charge jets with the crater walls in penetrating metals and brittle materials. *Int. J. Impact Engng* **29**, 385–390.
33. Dietz, P. (2001) Research into the use of polymeric film to enhance the safety of sideglass. *SAE Trans.: J. Mater. Manuf.* **110**, 782–785.
34. Haward, R. N. (1945) The behaviour of laminated and toughened glass under impact by a falling bolt. *J. Soc. Glass Technol.* **29**, 197–198.
35. Behr, R. A., Kremer, P. A., Dharani, L. R., Ji, F. S. and Kaiser, N. D. (1999) Dynamic strains in architectural laminated glass subjected to low velocity impacts from small projectiles. *J. Mater. Sci.* **34**, 5749–5756.
36. Flocker, F. W. and Dharani, L. R. (1997) Stresses in laminated glass subject to low velocity impact. *Engng Struct.* **19**, 851–856.
37. Flocker, F. W. and Dharani, L. R. (1998) Modeling interply debonding in laminated architectural glass subject to low velocity impact. *Struct. Engng Mech.* **6**, 485–496.
38. Flocker, F. W. and Dharani, L. R. (1998) Low velocity impact resistance of laminated architectural glass. *ASCE J. Architectural Engng* **4**, 12–17.
39. Ji, F. S., Dharani, L. R. and Behr, R. A. (1998) Damage probability in laminated glass subjected to low velocity small missile impacts. *J. Mater. Sci.* **33**, 4775–4782.
40. Grant, P. V., Cantwell, W. J., McKenzie, H. and Corkhill, P. (1998) The damage threshold of laminated glass structures. *Int. J. Impact Engng* **21**, 737–746.
41. Kaiser, N. D., Behr, R. A., Minor, J. E., Dharani, L. R., Ji, F. and Kremer, P. A. (2000) Impact resistance of laminated glass using sacrificial ply design concept. *ASCE J. Architectural Engng* **6**, 24–34.
42. Danaher, D. A., Johnson, W. S., Railsback, B. T. and Ziernicki, R. M. (2002) A new polycarbonate and glass laminate and its effects on the relationship between residual tensile stresses and impact resistance of windshields. *SAE Trans.: J. Mater. Manuf.* **111**, 786–801.
43. Buchar, J., Rolc, S., Voldrich, J., Lazar, M. and Starek, M. (2001) The development of the glass laminates resistant to the small arms fire. In: I. R. Crewther (ed) Proc. 19th Int. Symp. on Ballistics. Interlaken, Switzerland: 1439–1445.
44. Bless, S. J., Chen, T. and Russell, R. (2007) Impact of glass laminates. In: Proc. 23rd Int. Symp. on Ballistics, F. Gálvez, V. Sánchez-Gálvez (eds). Universidad Politécnica de Madrid, Madrid, Spain: 1503–1510.
45. Walley, S. M., Field, J. E., Blair, P. W. and Milford, A. J. (2004) The effect of temperature on the impact behaviour of glass/polycarbonate laminates. *Int. J. Impact Engng* **30**, 31–53.
46. Bless, S. (2010) Observations of ballistic impact damage in glass laminate. In: E. Buzaud, I. R. Ionescu and G. Z. Voyiadjis (eds) Materials under Extreme Loadings: Application to Penetration and Impact. Wiley, Hoboken, NJ: 87–99.
47. Bless, S. and Chen, T. (2010) Impact damage in layered glass. *Int. J. Fract.* **162**, 151–158.
48. Bobaru, F., Ha, Y. D. and Hu, W. (2012) Damage progression from impact in layered glass modeled with peridynamics. *Cent. Eur. J. Engng* **2**, 651–661.
49. Swab, J. J., LaSalvia, J. C., Gilde, G. A., Patel, P. J. and Motyka, M. J. (1999) Transparent armor ceramics: AlON and spinel. *Ceram. Engng Sci. Proc.* **20**, 79–84.
50. Strassburger, E., Patel, P., McCauley, J. W. and Templeton, D. W. (2005) Visualization of wave propagation and impact damage in a polycrystalline transparent ceramic: AlON. In: Proc. 22nd Int. Symp. on Ballistics, W. Flis and B. Scott (eds). DEStech Publications Inc., Lancaster, PA: 769–776.
51. McCauley, J. W., Patel, P., Chen, M. W., Gilde, G., Strassburger, E., Paliwal, P., Ramesh, K. T. and Dandekar, D. P. (2009) AlON: a brief history of its emergence and evolution. *J. Eur. Ceram. Soc.* **29**, 223–236.
52. Goldman, L. M., Twedt, R., Foti, R., Smith, M. and Sastri, S. A. (2009) Large-area AlON windows for reconnaissance and armor applications. *Proc. SPIE* **7302**, 730206.
53. Goldman, L. M., Foti, R., Smith, M., Kashalikar, U. and Sastri, S. (2010) AlON transparent armor. *Ceram. Engng Sci. Proc.* **30**, 225–232.
54. Goldman, L. M., Twedt, R., Balasubramanian, S. and Sastri, S. (2011) AlON optical ceramic transparencies for window, dome, and transparent armor applications. *Proc. SPIE* **8016**, 801608.
55. Alexander, C. S., Reinhart, W. D., Thornhill, T. F. and Chhabildas, L. C. (2010) Armor options: a comparison of the dynamic response of materials in the aluminum–oxide–aluminum nitride family. *Int. J. Appl. Ceram. Technol.* **7**, 587–594.
56. Grujicic, M., Bell, W. C. and Pandurangan, B. (2012) Design and material selection guidelines and strategies for transparent armor systems. *Mater. Design* **34**, 808–819.
57. Haque, B. Z., Kearney, M. M. and Gillespie Jr. J. W. (2012) Advances in protective personnel and vehicle armors. *Recent Patents Mater. Sci.* **5**, 105–136.
58. Strassburger, E., Hunzinger, M., Patel, P. and McCauley, J. W. (2013) Analysis of the fragmentation of AlON and spinel under ballistic impact. *Trans. ASME: J. Appl. Mech.* **80**, 031807.
59. Mott, N. F. (1977) Electrons in glass. *Contemp. Phys.* **18**, 225–245.
60. Field, J. E., Walley, S. M., Proud, W. G., Goldrein, H. T., Siviour, C. R. (2004) Review of experimental techniques for high rate deformation and shock studies. *Int. J. Impact Engng* **30**, 725–775.

© 2013 Wiley Publishing Ltd
doi: 10.1111/str.12075

61. Rumpf, H., Faulhaber, F. and Umhauer, H. (1967) Analyse der Brucherscheinungen in Glaskugeln und kreisrunden Glasscheiben. *Dechema Monograph.* **57**, 85–126.
62. Field, J. E. (1971) Dynamic fracture: its study and application. *Contemp. Phys.* **12**, 1–31.
63. Field, J. E. (1983) High-speed photography. *Contemp. Phys.* **24**, 439–459.
64. Glenn, L. A. (1976) The fracture of a glass half-space by projectile impact. *J. Mech. Phys. Solids* **24**, 93–106.
65. Bowden, F. P., Brunton, J. H., Field, J. E. and Heyes, A. D. (1967) Controlled fracture of brittle solids and interruption of electric current. *Nature* **216**, 38–42.
66. Jacobson, A. (1967) Bifurcation velocity of glassy materials. *Israel J. Technol.* **5**, 298–302.
67. Kalthoff, J. F. (1973) On the propagation direction of bifurcated cracks. In: G. C. Sih (ed) Dynamic Crack Propagation. Noordhoff International, Leyden, The Netherlands: 449–458.
68. Kobayashi, A., Ohtani, N. and Sato, T. (1978) Strain rate effects on viscoelastic crack bifurcation. *Engng Fract. Mech.* **10**, 75–79.
69. Ball, A. (1996) On the bifurcation of cone cracks in glass plates. *Philos. Mag. A* **73**, 1093–1103.
70. Field, J. E., Heyes A. D. (1965) The fracture of materials of high elastic moduli. In: Proceedings of the Seventh International Congress on High-speed Photography, O. Helwich (ed). Verlag Dr. Othmar Helwich, Zurich: 391–398.
71. Chaudhri, M. M. (2006) Explosive disintegration of thermally toughened sodalime glass and Prince Rupert's drops. *Phys. Chem. Glasses* **47**, 136–141.
72. Brodsley, L., Frank, C. and Steeds, J. W. (1986) Prince Rupert's drops. *Notes Records R. Soc. Lond.* **41**, 1–26.
73. Chaudhri, M. M. (1998) Crack bifurcation in disintegrating Prince Rupert's drops. *Philos. Mag. Letts* **78**, 153–158.
74. Chaudhri, M. M. (2009) The role of residual stress in a Prince Rupert's drop of sodalime glass undergoing a self-sustained and stable destruction/fracture wave. *Phys. Stat. Sol. A* **206**, 1410–1413.
75. Chaudhri, M. M. (2011) Self-sustained fracture waves in sodalime glass. *Mater. Sci. Forum* **662**, 95–104.
76. Chaudhri, M. M. (2011) Self-sustained fracture waves in a lead oxide–silica glass. *J. Appl. Phys.* **110**, 013523.
77. Chaudhri, M. M. and Chen, L. (1986) The catastrophic failure of thermally toughened tempered glass caused by small-particle impact. *Nature* **320**, 48–50.
78. Taylor, G. I. (1946) The testing of materials at high rates of loading. *J. Inst. Civil Engrs* **26**, 486–519.
79. Volterra, E. (1948) Alcuni risultati di prove dinamiche sui materiali (Some results on the dynamic testing of materials). *Rivista Nuovo Cimento* **4**, 1–28.
80. Kolsky, H. (1949) An investigation of the mechanical properties of materials at very high rates of loading. *Proc. Phys. Soc. Lond. B* **62**, 676–700.
81. Dannemann, K. A., Nicholls, A. E., Anderson, Jr. C. E., Chocron, S. and Walker, J. D. (2007) Response and characterization of confined borosilicate glass: Intact and damaged. In: Advances in Ceramic Armor. 2, L. P. Franks (ed). Wiley, Hoboken, NJ: 119–130.
82. Nie, X., Chen, W. W., Sun, X. and Templeton, D. W. (2007) Dynamic failure of borosilicate glass under compression/shear loading experiments. *J. Amer. Ceram. Soc.* **90**, 2556–2562.
83. Chocron, S., Dannemann, K. A., Walker, J. D., Nicholls, A. E. and Anderson, Jr. C. E. (2009) Static and dynamic confined compression of borosilicate glass. In: Proc. 9th Int. Conf. on the Mechanical and Physical Behaviour of Materials under Dynamic Loading (DYMAT 2009). EDP Sciences, Les Ulis, France: 67–72.
84. Nie, X. and Chen, W. (2013) High-rate progressive failure of borosilicate glass under mechanical confinement at high temperatures. *Exper. Mech.* **53**, 67–75.
85. Taylor, G. I. (1948) The use of flat ended projectiles for determining yield stress. 1: Theoretical considerations. *Proc. R. Soc. Lond. A* **194**, 289–299.
86. Forde, L. C., Proud, W. G. and Walley, S. M. (2009) Symmetrical Taylor impact studies of copper. *Proc. R. Soc. A* **465**, 769–790.
87. Forde, L. C., Walley, S. M., Peyton-Jones, M., Proud, W. G., Cullis, I. G., Church, P. D. (2009) The use of symmetric Taylor impact to validate constitutive models for an fcc metal (copper) and a bcc alloy (RHA steel). In: Proc. 9th Int. Conf. on the Mechanical and Physical Behaviour of Materials under Dynamic Loading (DYMAT 2009). EDP Sciences, Les Ulis, France, 1245–1250.
88. Hutchings, I. M. (1978) Estimation of yield stress in polymers at high strain rates using G.I. Taylor's impact technique. *J. Mech. Phys. Solids* **26**, 289–301.
89. Brar, N. S., Bless, S. J. and Rosenberg, Z. (1988) Brittle failure of ceramic rods under dynamic compression. *J. Phys. France* **49**(C3), 607–612.
90. Bless, S. J., Brar, N. S., Rosenberg, Z. (1990) Failure of ceramic and glass rods under dynamic compression. In: Shock Compression of Condensed Matter—1989, S. C. Schmidt, J. N. Johnson and L. W. Davidson (eds). Elsevier, Amsterdam: 939–942.
91. Brar, N. S., Bless, S. J., Rosenberg, Z. (1991) Impact-induced failure waves in glass bars and plates. *Appl. Phys. Letts* **59**, 3396–3398.
92. Brar, N. S., Bless, S. J. (1992) Dynamic fracture and failure mechanisms of ceramic bars. In: M. A. Meyers, L. E. Murr and K. P. Staudhammer (eds) Shock-wave and High-strain-rate Phenomena in Materials. Marcel-Dekker, New York: 1041–1050.
93. Murray, N. H., Bourne, N. K., Field, J. E., Rosenberg, Z. (1998) Symmetrical Taylor impact of glass bars. In: Shock Compression of Condensed Matter—1997, S. C. Schmidt, D. P. Dandekar and J. W. Forbes (eds). American Institute of Physics, Woodbury, New York: 533–536.
94. Radford, D. D., Willmott, G. R., Walley, S. M., Field, J. E. (2003) Failure mechanisms in ductile and brittle materials during Taylor impact. *J. Phys. IV France* **110**, 687–692.
95. Radford, D. D., Willmott, G. R. and Field, J. E. (2004) The effect of structure on failure front velocities in glass rods. In: M. D. Furnish, Y. M. Gupta and J. W. Forbes (eds) Shock Compression of Condensed Matter—2003. American Institute of Physics, Melville NY: 755–758.
96. Willmott, G. R., Radford, D. D. (2005) Taylor impact of glass rods. *J. Appl. Phys.* **97**, 093522.
97. Baird, K. M. (1947) Shock wave in glass. *Nature* **160**, 24–25.
98. Kolsky, H., Shi, Y. Y. (1958) Fractures produced by stress pulses in glass-like solids. *Proc. Phys. Soc. Lond.* **72**, 447–453.

© 2013 Wiley Publishing Ltd | ***Strain*** (2014) **50**, 470–500
doi: 10.1111/str.12075

99. Kolsky, H. (1959) Fractures produced by stress waves. In: B. L. Averbach, D. K. Felbeck, G. T. Hahn and D. A. Thomas (eds) Fracture. John Wiley, New York: 281–296.
100. Kolsky, H. (1976) The waves generated by brittle fracture in glass. *Trans. Soc. Rheology* **20**, 441–454.
101. Kachanov, L. M. (1976) Brittle fracture of a rod under longitudinal impact. *Engng Fract. Mech.* **8**, 255–259.
102. Kuzmin, V. S. and Nikiforovskii, V. S. (1980) Dynamic fracturing of glass rods. *J. Appl. Mech. Tech. Phys.* **21**, 711–716.
103. Ishii, T., Matsushita, M. (1992) Fragmentation of long thin glass rods. *J. Phys. Soc. Jpn* **61**, 3474–3477.
104. Ching, E. S. C., Lui, S. L., Xia, K.-Q. (2000) Energy dependence of impact fragmentation of long glass rods. *Physica A* **287**, 83–90.
105. Chapman, D. J., Radford, D. D., Reynolds, M. and Church, P. D. (2005) Shock induced void nucleation during Taylor impact. *Int. J. Fract.* **134**, 41–57.
106. Marsh, S. P. (1980) LASL Shock Hugoniot Data. University of California Press, Berkeley, California.
107. Viard, J. (1959) Courbe d'Hugoniot de la silice vitreuse et cristallisation sous choc. *C.R. Acad. Sci. Paris* **249**, 820–822.
108. Mallory, H. D., McEwan, W. S. (1961) Transparency of glass and certain plastics under shock attack. *J. Appl. Phys.* **32**, 2421–2424.
109. Dremin, A. N., Adadurov, G. (1964) The behavior of glass under dynamic loading. *Sov. Phys. Solid State* **6**, 1379–1384.
110. Deribas, A. A., Dobretsov, N. L., Kudinov, V. M., Zyuzin, N. I. (1966) Shock compression of SiO_2 powders. *Dokl. Acad. Sci. USSR: Earth Science Sections* **168**, 127–130.
111. Arndt, J., Hornemann, H. and Müller, W. F. (1971) Shock wave densification of silica glass. *Phys. Chem. Glasses* **12**, 1–7.
112. Kanel, G. I. and Molodets, A. M. (1976) Behavior of type K-8 glass in dynamic compression and subsequent unloading. *Sov. Phys. Tech. Phys.* **21**, 226–232.
113. Kanel, G. I., Molodets, A. M., Dremin, A. N. (1977) Investigation of singularities of glass strain under intense compression waves. *Combust. Explos. Shock Waves* **13**, 772–777.
114. Bourne, N. K., Millett, J. C. F., Field, J. E. (1999) On the strength of shocked glasses. *Proc. R. Soc. Lond. A* **455**, 1275–1282.
115. Maloy, S. A., Gray, III G. T., Cady, C. M., Rutherford, R. W. and Hixson, R. S. (2004) The influence of explosive-driven 'Taylor-wave' shock prestraining on the structure/property behavior of 304 stainless steel. *Metall. Mater. Trans. A* **35**, 2617–2624.
116. Yaziv, D., Bless, S. J. and Rosenberg, Z. (1985) Study of spall and recompaction of ceramics using a double-impact technique. *J. Appl. Phys.* **58**, 3415–3418.
117. Rosenberg, Z., Brar, N. S. and Bless, S. J. (1990) Determination of the strength of shock loaded ceramics using double impact techniques. In: Shock Compression of Condensed Matter—1989, S. C. Schmidt, J. N. Johnson and L. W. Davidson (ed). Elsevier, Amsterdam: 385–388.
118. Yeshurun, Y., Rosenberg, G. and Rosenberg, Z. (1986) Measurements of compressive and tensile waves in a shock loaded Pyrex glass. In: Shock Waves in Condensed Matter, Y. M. Gupta (ed). Plenum Press, New York: 431–435.
119. Bless, S. J., Brar, N. S. and Rosenberg, Z. (1988) Strength of soda lime glass under shock compression. In: Shock Waves in Condensed Matter 1987, S. C. Schmidt and N. C. Holmes (eds). North Holland, Amsterdam: 309–312.
120. Rosenberg, Z., Marmor, E. and Mayseless, M. (1990) On the hydrodynamic theory of long-rod penetration. *Int. J. Impact Engng* **10**, 483–486.
121. Rasorenov, S. V., Kanel, G. I., Fortov, V. E., Abasehov, M. M. (1991) The fracture of glass under high pressure impulsive loading. *High Press. Res.* **6**, 225–232.
122. Kanel, G. I., Rasorenov, S. V. and Fortov, V. E. (1992) The failure waves and spallations in homogeneous brittle materials. In: Shock Compression of Condensed Matter—1991, S. C. Schmidt, R. D. Dick, J. W. Forbes and D. G. Tasker (ed). Elsevier, Amsterdam: 451–454.
123. Orphal, D. L., Anderson, Jr. C. E., Behner, T. and Templeton, D. W. (2009) Failure and penetration response of borosilicate glass during multiple short-rod impact. *Int. J. Impact Engng* **36**, 1173–1181.
124. Brar, N. S., Rosenberg, Z. and Bless, S. J. (1991) Spall strength and failure waves in glass. *J. Phys. IV France* **1**(C3), 639–644.
125. Brar, N. S. and Bless, S. J. (1992) Failure waves in glass under dynamic compression. *High Press. Res.* **10**, 773–784.
126. Brar, N. S. and Espinosa, H. D. (1998) A review of micromechanics of failure waves in silicate glasses. *Chem. Phys. Rep.* **17**, 317–342.
127. Brar, N. S. (2000) Failure waves in glass and ceramics under shock compression. In: Shock Compression of Condensed Matter—1999, (M. D. Furnish, L. C. Chhabildas and R. S. Hixson) (eds). American Institute of Physics, Melville, New York: 601–606.
128. Clifton, R. J. (1993) Analysis of failure waves in glasses. *Appl. Mech. Rev.* **46**, 540–546.
129. Raiser, G., Clifton, R. J. (1994) Failure waves in uniaxial compression of an aluminosilicate glass. In: S. C. Schmidt, J. W. Shaner, G. A. Samara and M. Ross (eds) High Pressure Science and Technology 1993. American Institute of Physics, New York: 1039–1042.
130. Bourne, N. K., Rosenberg, Z. and Field, J. E. (1995) High-speed photography of compressive failure waves in glasses. *J. Appl. Phys.* **78**, 3736–3739.
131. Bourne, N. K., Rosenberg, Z. and Millett, J. C. F. (1996) The plate impact response of three glasses. In: Structures under Shock and Impact IV, (N. Jones, C. A. Brebbia, A. J. Watson) (eds). Computational Mechanics Publications, Southampton: 553–562.
132. Bourne, N. K., Millett, J. C. F. and Rosenberg, Z. (1996) The shock wave response of a filled glass. *Proc. R. Soc. Lond. A* **452**, 1945–1951.
133. Bourne, N. K., Millett, J. C. F. and Rosenberg, Z. (1996) Failure in a shocked high-density glass. *J. Appl. Phys.* **80**, 4328–4331.
134. Bourne, N. K. and Rosenberg, Z. (1996) The dynamic response of soda-lime glass. In: S. C. Schmidt and W. C. Tao (eds) Shock Compression of Condensed Matter 1995. American Institute of Physics, Woodbury, New York: 567–572.
135. Bourne, N. K., Millett, J. C. F., Rosenberg, Z. (1997) On the origin of failure waves in glass. *J. Appl. Phys.* **81**, 6670–6674.
136. Espinosa, H. D. and Xu, Y. P. (1997) Micromechanics of failure waves in glass. 1: Experiments. *J. Amer. Ceram. Soc.* **80**, 2061–2073.

© 2013 Wiley Publishing Ltd |
doi: 10.1111/str.12075

137. Espinosa, H. D., Xu, Y. P., Brar, N. S. (1997) Micromechanics of failure waves in glass. 2: Modeling. *J. Amer. Ceram. Soc.* **80**, 2074–2085.
138. He, H. L., Jin, X. G., Jing, F. Q. and Kanel, G. I. (1997) Dynamic failure of shock-loaded glass. *Chinese Phys. Letts* **14**, 538–541.
139. Clifton, R. J., Mello, M. and Brar, N. S. (1998) Effect of shear on failure waves in soda lime glass. In: Shock Compression of Condensed Matter—1997, S. C. Schmidt, D. P. Dandekar and J. W. Forbes (eds). American Institute of Physics, Woodbury, New York: 521–524.
140. Kanel, G. I., Razorenov, S. V., Utkin, A. V., He, H. L., Jing, F. Q. and Jin, X. G. (1998) Influence of the load conditions on the failure wave in glasses. *High Press. Res.* **16**, 27–44.
141. Partom, Y. (1998) Modeling failure waves in glass. *Int. J. Impact Engng* **21**, 791–799.
142. Chen, Z. and Xin, X. (1999) An analytical and numerical study of failure waves. *Int. J. Solids Structures* **36**, 3977–3991.
143. Abeyaratne, R. and Knowles, J. K. (2000) A phenomenological model for failure waves in glass. *Shock Waves* **10**, 301–305.
144. Cazamias, J. U., Fiske, P. S. and Bless, S. J. (2001) Sound speeds of post-failure wave glass. In: Fundamental Issues and Applications of Shock-wave and High-strain-rate Phenomena, K. P. Staudhammer, L. E. Murr and M. A. Meyers (eds). Elsevier, New York: 173–179.
145. Simha, C. H. M., Gupta, Y. M. (2004) Time-dependent inelastic deformation of shocked sodalime glass. *J. Appl. Phys.* **96**, 1880–1890.
146. Bless, S. and Brar, N. (2007) Failure waves and their effects on penetration mechanics in glass and ceramics. In: Shock Wave Science and Technology Reference Library. 2: Solids I, Y. Horie (ed). Springer, Berlin: 105–141.
147. Bless, S. J. (2010) Failure waves and their possible roles in determining penetration resistance of glass. *Int. J. Appl. Ceram. Technol.* **7**, 400–408.
148. Medin, S. A. and Parshikov, A. N. (2012) Modeling of failure wave propagation in impact compression of brittle materials: glasses. *Mech. Solids* **47**, 242–251.
149. Rosenberg, Z., Bourne, N. K. and Millett, J. C. F. (1996) Direct measurements of strain in shock-loaded glass specimens. *J. Appl. Phys.* **79**, 3971–3974.
150. Cagnoux, J. (1982) Shock-wave compression of a borosilicate glass up to 170 kbar. *AIP Conf. Ser.* **78**, 392–396.
151. Bridgman, P. W. and Simon, I. (1953) Effects of very high pressures on glass. *J. Appl. Phys.* **24**, 405–413.
152. Deribas, A., Dobretsov, N., Kudinov, V., Maly, V., Serebrjakov, A. and Staver, A. (1968) Shock wave compression of some inorganic compositions. In: Behaviour of Dense Media under High Dynamic Pressures. Gordon and Breach, New York: 385–388.
153. Dobretsov, N. L., Deribas, A. A. and Maly, V. I. (1970) Shock compression of powdered SiO_2, Mg_2SiO_4, $ZrSiO_4$ and other materials. *Phys. Earth Planet. Inter.* **3**, 348–355.
154. Hagan, J. T. (1980) Shear deformation under pyramidal indentations in soda-lime glass. *J. Mater. Sci.* **15**, 1417–1424.
155. Orphal, D. L., Kozhushko, A. A. and Sinani, A. B. (2000) Possible detection of failure wave velocity in SiC using hypervelocity penetration experiments. In: M. D. Furnish, L. C. Chhabildas and R. S. Hixson (eds) Shock Compression of Condensed Matter—1999. American Institute of Physics, Melville, New York: 577–580.
156. Plekhov, O. A., Eremeev, D. N. and Naimark, O. B. (2000) Failure wave as resonance excitation of collective burst modes of defects in shocked brittle materials. *J. Phys. IV France*, **10**(Pr. 9), 811–816.
157. Anderson, Jr. C. E., Orphal, D. L. and Templeton, D. W. (2004) Re-examination of the requirements to detect the failure wave velocity in SiC using penetration experiments. In: Shock Compression of Condensed Matter—2003, M. D. Furnish, Y. M. Gupta and J. W. Forbes (eds). American Institute of Physics, Melville NY: 707–710.
158. Anderson, C. E., Orphal, D. L., Behner, T., Hohler, V. and Templeton, D. W. (2006) Re-examination of the evidence for a failure wave in SiC penetration experiments. *Int. J. Impact Engng* **33**, 24–34.
159. Staehler, J. M., Predebon, W. W. and Pletka, B. J. (1994) The response of a high purity alumina to plate impact testing. In: High Pressure Science and Technology 1993, S. C. Schmidt, J. W. Shaner, G. A. Samara and M. Ross (eds). American Institute of Physics, New York: 745–748.
160. Murray, N. H., Millett, J. C. F., Proud, W. G. and Rosenberg, Z. (2000) Issues surrounding lateral stress measurements in alumina ceramics. In: Shock Compression of Condensed Matter—1999, M. D. Furnish, L. C. Chhabildas and R. S. Hixson (eds). American Institute of Physics, Melville, New York: 581–584.
161. Murray, N. H. and Proud, W. G. (2001) Measurement of lateral stress and spall strength in ceramics. In: Fundamental Issues and Applications of Shock-wave and High-strain-rate Phenomena, K. P. Staudhammer, L. E. Murr, M. A. Meyers (eds). Elsevier, New York: 151–156.
162. Grady, D. E. (1998) Shock wave compression of brittle solids. *Mech. Mater.* **29**, 181–203.
163. Marom, H., Sherman, D. and Rosenberg, Z. (2000) Decay of elastic waves in alumina. *J. Appl. Phys.* **88**, 5666–5670.
164. Kozhushko, A. A., Orphal, D. L., Sinani, A. B. and Franzen, R. R. (1999) Possible detection of failure wave velocity using hypervelocity penetration experiments. *Int. J. Impact Engng* **23**, 467–476.
165. Satapathy, S., Bless, S., Ivanov S. M. (1999) The effects of failure wave on penetration resistance of glass. In: Proc. 18th. Int. Symp. on Ballistics, W. G. Reinecke (ed). Technomic Publishing Company, Inc., Lancaster, Pennsylvania: 1159–1167.
166. Zilberbrand, E. L., Vlasov, A. S., Cazamias, J. U., Bless, S. J. and Kozhushko, A. A. (1999) Failure wave effects in hypervelocity penetration. *Int. J. Impact Engng* **23**, 995–1002.
167. Bourne, N. K. (2008) The relation of failure under 1D shock to the ballistic performance of brittle materials. *Int. J. Impact Engng* **35**, 674–683.
168. Radford, D. D., Proud, W. G. and Field, J. E. (2002) The deviatoric response of three dense glasses under shock loading conditions. In: Shock Compression of Condensed Matter—2001, M. D. Furnish, N. N. Thadhani and Y. Horie (eds). American Institute of Physics, Melville, NY: 807–810.
169. Grujicic, M., Pandurangan, B., Bell, W. C., Cheeseman, B. A., Patel, P. and Gazonas, G. A. (2011) Molecular-level analysis of shock-wave physics and derivation of the

© 2013 Wiley Publishing Ltd
doi: 10.1111/str.12075

Hugoniot relations for sodalime glass. *J. Mater. Sci.* **46**, 7298–7312.
170. Grujicic, M., Pandurangan, B., Zhang, Z., Bell, W. C., Gazonas, G. A., Patel, P. and Cheeseman, B. A. (2012) Molecular level analysis of shock-wave physics and derivation of the Hugoniot relations for fused silica. *J. Mater. Engng Perform.* **21**, 823–836.
171. Grujicic, M., Bell, W. C., Pandurangan, B., Cheeseman, B. A., Fountzoulas, C. and Patel, P. (2012) Molecular level simulations of shock generation and propagation in sodalime glass. *J. Mater. Engng Perform.* **21**, 1580–1590.
172. Roesler, F. C. (1956) Brittle fractures near equilibrium. *Proc. Phys. Soc. Lond. B* **69**, 981–992.
173. Benbow, J. J. (1960) Cone cracks in fused silica. *Proc. Phys. Soc. Lond.* **75**, 697–699.
174. Frank, F. C. and Lawn, B. R. (1967) On the theory of Hertzian fracture. *Proc. R. Soc. Lond. A* **299**, 291–306.
175. Lawn, B. R. and Wilshaw, T. R. (1975) Review: indentation fracture —principles and applications. *J. Mater. Sci.* **10**, 1049–1081.
176. Hagan, J. T. (1979) Cone cracks around Vickers indentations in fused silica glass. *J. Mater. Sci.* **14**, 462–466.
177. Li, Y. and Hills, D. A. (1991) The Hertzian cone crack. *Trans. ASME: J. Appl. Mech.* **58**, 120–127.
178. Lawn, B. (1993) Fracture of Brittle Solids (2nd edn.), Chapter 8: Indentation fracture. Cambridge University Press, Cambridge.
179. Licht, V., Hülsmeier, P. and Fett, T. (2004) Probability of cone crack initiation due to spherical contact loading. *J. Eur. Ceram. Soc.* **24**, 2907–2916.
180. Yan, J., Karlsson, A. M. and Chen, X. (2007) On internal cone cracks induced by conical indentation in brittle materials. *Engng Fract. Mech.* **74**, 2535–2546.
181. Lawn, B. R., Wilshaw, T. R. and Hartley, N. E. W. (1974) A computer simulation study of Hertzian cone crack growth. *Int. J. Fract.* **10**, 1–16.
182. Zeng, K., Breder, K. and Rowcliffe, D. J. (1992) The Hertzian stress field and formation of cone cracks. 1: Theoretical approach. *Acta Metall. Mater.* **40**, 2595–2600.
183. Zeng, K., Breder, K. and Rowcliffe, D. J. (1992) The Hertzian stress field and formation of cone cracks. 2: Determination of fracture toughness. *Acta Metall. Mater.* **40**, 2601–2605.
184. Hertz, H. (1882) Über die Berührung fester elastischer Körper. *J. Reine Angew. Math.* **92**, 156–171.
185. Hertz, H. (1896) On the contact of elastic solids. In: Miscellaneous Papers by Heinrich Hertz, D. E. Jones and G. A. Schott (eds). Macmillan, London: 146–162.
186. Hertz, H. (1896) On the contact of rigid elastic solids and on hardness. In: Miscellaneous Papers by Heinrich Hertz, D. E. Jones, G. A. Schott (eds). Macmillan, London: 163–183.
187. Huber, M. T. (1904) Zur Theorie der Berührung fester elastischer Körper. *Ann. Phys. (Leipzig)* **14**, 153–163.
188. Fuchs, S. (1913) Hauptspannungstrajektorien bei der Berührung einer Kugel mit einer Platte. *Phys. Z.* **14**, 1282–1285.
189. Love, A. E. H. (1920) Solution of the problem of the pressure between two bodies in contact. In: A Treatise on the Mathematical Theory of Elasticity (Third Edition). Cambridge University Press, Cambridge: 193–196.
190. Chaudhri, M. M. and Walley, S. M. (1978) Damage to glass surfaces by the impact of small glass and steel spheres. *Philos. Mag. A* **37**, 153–165.
191. Knight, C. G., Swain, M. V. and Chaudhri, M. M. (1977) Impact of small steel spheres on glass surfaces. *J. Mater. Sci.* **12**, 1573–1586.
192. Chaudhri, M. M. and Brophy, P. A. (1980) Single particle impact damage of fused silica. *J. Mater. Sci.* **15**, 345–352.
193. Chaudhri, M. M. (1985) High speed photographic investigations of the dynamic localised loading of some oxide glasses. In: Strength in Inorganic Glasses, C. R. Kurkjian (ed). Plenum, New York: 87–113.
194. Chaudhri, M. M. and Kurkjian, C. R. (1986) Impact of small steel spheres on the surfaces of 'normal' and 'anomalous' glasses. *J. Amer. Ceram. Soc.* **69**, 404–410.
195. Chaudhri, M. M. and Chen, L. (1989) The orientation of the Hertzian cone crack in soda-lime glass formed by oblique dynamic and quasi-static loading with a hard sphere. *J. Mater. Sci.* **24**, 3441–3448.
196. Chaudhri, M. M., Smith, A. L. (1990) Damage to polymer-coated glass surfaces by small particle impact. *Proc. SPIE* **1358**, 683–691.
197. Kim, M.-S., Shin, H.-S. and Lee, H.-C. (2003) The effects of back plate materials on perfect cone formation in impact-loaded sodalime glass. *Int. J. Impact Engng* **28**, 281–290.
198. Kim, M.-S., Shin, H.-S., Lee, H.-C. and Kim, H.-J. (2004) Effects of impact angle on cone crack formation in impact-loaded sodalime glass. *Key Engng Mater.* **261**, 319–324.
199. Suh, C. M., Kim, D. K. and Lee, M. H. (2006) A study on damage behavior of glass by oblique impact of steel ball. *Int. J. Mod. Phys. B* **20**, 4291–4296.
200. Kocer, C. and Collins, R. E. (1998) Angle of Hertzian cone cracks. *J. Amer. Ceram. Soc.* **81**, 1736–1742.
201. Oh, S. Y. and Shin, H. S. (2005) Effect of particle impact velocity on cone crack shape in ceramic material. *Key Engng Mater.* **297**, 1321–1326.
202. Johnson, K. L., O'Connor, T. J. and Woodward, A. C. (1973) The effect of the indenter elasticity on the Hertzian fracture of brittle materials. *Proc. R. Soc. Lond. A* **334**, 95–117.
203. Shishacov, N. (1938) Mosiac blocks of silicate glasses. *Tech. Phys. USSR* **5**, 666–675.
204. Shand, E. B. (1954) Experimental study of fracture of glass. 1: The fracture process. *J. Amer. Ceram. Soc.* **37**, 52–59.
205. Shand, E. B. (1954) Experimental study of fracture of glass. 2: Experimental data. *J. Amer. Ceram. Soc.* **37**, 559–572.
206. Field, J. E. (1966) Stress waves, deformation and fracture caused by liquid impact. *Phil. Trans. R Soc. Lond. A* **260**, 86–93.
207. Warren, P. D., Hills, D. A. and Roberts, S. G. (1994) Influence of surface cracks on Hertzian fracture. *J. Hard Mater.* **5**, 213–227.
208. Warren, P. D., Hills, D. A. and Roberts, S. G. (1994) Surface flaw distributions in brittle materials and Hertzian fracture. *J. Mater. Res.* **9**, 3194–3202.
209. Field, J. E., Sun, Q. and Townsend, D. (1989) Ballistic impact of ceramics. *Inst. Phys. Conf. Ser.* **102**, 387–393.
210. Sun, Q. and Field, J. E. (1992) Spherical projectile impact on aluminas. In: G. Zhang, S. Huang (eds) Proc. 2nd. Int. Symp. on Intense Dynamic Loading and Its Effects. Sichuan University Press, Chengdu, P.R. China, 384–390.
211. Haward, R. N. (1944) The behaviour of laminated and toughened glass under static bending and impact at different velocities. *J. Soc. Glass Technol.* **28**, 133–151, 469–471.

© 2013 Wiley Publishing Ltd |

212. Bless, S. J. and Hartman, D. R. (1989) Ballistic penetration of S-2 glass laminates. In: Proc. 21st Int. SAMPE Technical Conf, R. Wegman, E. Hogan and H. Kliger (eds). Society for the Advancement of Material and Process Engineering, Covina, CA: 852–866.
213. Richards, M., Clegg, R. and Howlett, S. (1999) Ballistic performance assessment of glass laminates through experimental and numerical investigation. In: Proc. 18th. Int. Symp. on Ballistics, W. G. Reinecke (ed). Technomic Publishing Company, Inc., Lancaster, Pennsylvania: 1123–1130.
214. Hu, W., Wang, Y., Yu, J., Yen, C.-F. and Bobaru, F. (2013) Impact damage on a thin glass plate with a thin polycarbonate backing. *Int. J. Impact Engng* **62**, 152–165.
215. Factor, A. and Chu, M. L. (1980) The role of oxygen in the photo-ageing of bisphenol-A polycarbonate. *Polym. Degrad. Stab.* **2**, 203–223.
216. Bubeck, R. A., Bales, S. E. and Lee, H. D. (1984) Changes in yield and deformation of polycarbonates caused by physical aging. *Polym. Engng Sci.* **24**, 1142–1148.
217. Clark, D. T. and Munro, H. S. (1984) Surface and bulk aspects of the natural and artificial photoageing of bisphenol-A polycarbonate as revealed by ESCA and difference UV spectroscopy. *Polym. Degrad. Stab.* **8**, 195–211.
218. Hill, A. J., Heater, K. J. and Keller, A. (1990) The effects of physical aging in polycarbonate. *J. Polym. Sci. B: Polym. Phys.* **28**, 387–405.
219. Huu, C. H. and Vu-Khanh, T. (2003) Effects of physical aging on yielding kinetics of polycarbonate. *Theor. Appl. Fract. Mech.* **40**, 75–83.
220. Senden, D. J. A., Engels, T. A. P., Söntjens, S. H. M. and Govaert, L. E. (2012) The effect of physical aging on the embrittlement of steam-sterilized polycarbonate. *J. Mater. Sci.* **47**, 6043–6046.
221. Bowden, F. P. and Field, J. E. (1964) The brittle fracture of solids by liquid impact, by solid impact and by shock. *Proc. R. Soc. Lond. A* **282**, 331–352.
222. Aenlle M. L. and Pelayo F. (2012) Frequency response of laminated glass elements: Analytical modeling and effective thickness. *Appl. Mech. Rev.* **65**, 020802.
223. Johnson, W. (1986) Historical and present-day references concerning impact on wood. *Int. J. Impact Engng* **4**, 161–174.
224. Reid, S. R. (1994) Impact energy absorption mechanisms in the crushing and indentation of wood. In: Z. Zheng and Q. Tan (eds) Proc. IUTAM Symp. on Impact Dynamics. Peking University Press, Beijing, China: 390–406.
225. Renaud, M., Rueff, M. and Rocaboy, A. C. (1996) Mechanical behavior of saturated wood under compression. 1: Behavior of wood at high rates of strain. *Wood Sci. Technol.* **30**, 153–164.
226. Renaud, M., Rueff, M. and Rocaboy, A. C. (1996) Mechanical behavior of saturated wood under compression. 2: Behavior of wood at low rates of strain. Some effects of compression on wood structure. *Wood Sci. Technol.* **30**, 237–243.
227. Itoh, S., Nagano, S. and Liu, Z. (1998) Underwater shock wave loading on wood. In: Structures under Shock and Impact V, N. Jones, D. G. Talaslidis, C. A. Brebbia and G. D. Manolis (eds). Computational Mechanics Publications, Southampton, UK: 435–444.
228. Buchar, J., Severa, L., Lazar, M., Rolc, S., Cech, V. and Lisy, J. (1999) The performance of wood plates under ballistic impact. In: Proc. 18th. Int. Symp. on Ballistics, W. G. Reinecke (ed). Technomic Publishing Company, Inc., Lancaster, Pennsylvania: 716–723.
229. Buchar, J., Severa, L. and Havlicek, V. (1999) The response of wood plates to high velocity impact. *Acta Univ. Agric. Silv. Mendel. Brun.* **47**(1), 31–37.
230. Buchar, J., Rolc, S., Lisy, J., Schwengmeier, J. (2001) Model of the wood response to the high velocity of loading. In: Proc. 19th Int. Symp. on Ballistics, I. R. Crewther (ed). RUAG Land Systems, Interlaken, Switzerland 1447–1453.
231. Buchar J., Severa L., Havlicek M. and Rolc S. (2000) Response of wood to explosive loading. *J. Phys. IV France* **10**(Pr. 9), 529–534.
232. Bolshakov, A. P., Balakshina, M. A., Gerdyukov, N. N., Zotov, E. V., Muzyrya, A. K., Plotnikov, A. F., Novikov, S. A., Sinitsyn, V. A., Shestakov, D. I. and Shcherbak, Y. I. (2001) Damping properties of Sequoia, Birch, Pine, and Aspen under shock loading. *J. Appl. Mech. Tech. Phys.* **42**, 202–210.
233. Buchar, J., Krivanek, I. and Severa, L. (2001) High strain rate behaviour of wood. In: New Experimental Methods in Material Dynamics and Impact, W. K. Nowacki and J. R. Klepaczko (eds). Institute of Fundamental Technological Research, Warsaw, Poland: 357–362.
234. Saxe, T. J., Behr, R. A., Minor, J. E., Kremer, P. A. and Dharani, L. R. (2002) Effects of missile size and glass type on impact resistance of 'sacrificial ply' laminated glass. *ASCE J. Architectural Engng* **8**, 24–39.
235. Bragov, A. M., Lomunov, A. K., Sergeichev, I. V. and Gray, III G. T. (2006) Dynamic behaviour of birch and sequoia at high strain rates. In: Shock Compression of Condensed Matter—2005, M. D. Furnish, M. Elert, T. P. Russell and C. T. White (eds). American Institute of Physics, Melville, NY: 1511–1514.
236. Takemoto, A., Maehara, H. and Itoh, S. (2006) Efficient using of wood by underwater shock wave. *Trans. Mater. Res. Soc. Jpn* **31**, 989–992.
237. Takemoto, A., Kuroda, K., Iyama, H. and Itoh, S. (2008) On the destruction of the cell wall of plants and its mechanism by the shock wave. *Int. J. Multiphys.* **2**, 165–170.
238. Holmgren, S. E., Svensson, B. A., Gradin, P. A. and Lundberg, B. (2008) An encapsulated split Hopkinson pressure bar for testing of wood at elevated strain rate, temperature, and pressure. *Exper. Techniq.* **32**(5), 44–50.
239. Allazadeh, M. R. and Wosu, S. N. (2012) High strain rate compressive tests on wood. *Strain* **48**, 101–107.
240. Bowden, F. P. and Brunton, J. H. (1961) The deformation of solids by liquid impact at supersonic speeds. *Proc. R. Soc. Lond. A* **263**, 433–450.
241. Matthewson, M. J. and Gorham, D. A. (1980) An oblique impact anomaly in high-velocity liquid impact on glass. *J. Mater. Sci.* **15**, 1518–1520.
242. Hand, R. J. and Field, J. E. (1990) Liquid impact on toughened glasses. *Engng Fract. Mech.* **37**, 293–311.
243. Barr, K. and Steeger, E. J. (1957) Supersonic rain erosion testing of missile radomes. *Jet Propulsion* **27**, 1034–1037.
244. Fyall, A. A. (1970) Rain erosion: a special radome problem. In: Radome Engineering Handbook: Design and Principles, J. D. Walton (ed). Dekker, New York: 461–562.
245. Smith, D. G. and Kinslow, R. (1977) Simulating rain impact damage to supersonic missile radomes. *J. Test. Eval.* **5**, 75–83.
246. Matthewson, M. J. and Gorham, D. A. (1981) An investigation of the liquid impact properties of a GFRP radome material. *J. Mater. Sci.* **16**, 1616–1626.

© 2013 Wiley Publishing Ltd | ***Strain*** (2014) **50**, 470–500
doi: 10.1111/str.12075

247. Adler, W. F. (1987) Development of design data for rain impact damage in infrared-transmitting windows and radomes. *Opt. Engng* **26**, 143–151.
248. Slikkerveer, P. J., Verspui, M. and Skerka, E. (1999) Erosion and damage by hard spherical particles on glass. *J. Amer. Ceram. Soc.* **82**, 3173–3178.
249. Taylor, E. W. (1950) The plastic deformation of optical glass. *J. Soc. Glass Technol.* **34**, 69–76.
250. Taylor, E. W. (1949) Plastic deformation of optical glass. *Nature* **163**, 323.
251. Diehl, W. and Schulze, R. (1957) Thermische, plastische Nachwirkungen an Vickerseindrücken in Glas. *Z. Angew. Phys.* **9**, 251–253.
252. Marsh, D. M. (1964) Plastic flow in glass. *Proc. R. Soc. Lond. A* **279**, 420–435.
253. Marsh, D. M. (1964) Plastic flow and fracture of glass. *Proc. R. Soc. Lond. A* **282**, 33–43.
254. Peter, K. (1964) Sprödbruch und Mikroplastizität von Glas in Eindruckversuchen. *Glastech. Berichte* **37**, 333–345.
255. Evers, M. (1967) Plastische Verformung von Glas mit Diamanteindrücken. *Glastech. Berichte* **40**, 41–43.
256. Ernsberger, F. M. (1968) Role of densification in deformation of glasses under point loading. *J. Amer. Ceram. Soc.* **51**, 545–547.
257. Peter, K. W. (1970) Densification and flow phenomena of glasses in indentation experiments. *J. Non-Cryst. Solids* **5**, 103–115.
258. Ernsberger, F. M. (1977) Mechanical properties of glass. *J. Non-Cryst. Solids* **25**, 295–321.
259. Hagan, J. T. (1979) Micromechanics of crack nucleation during indentations. *J. Mater. Sci.* **14**, 2975–2980.
260. Guillemet, C. (1995) Fracture et plasticité des verres. *Rev. Métall.* **92**, 253–263.
261. Sehgal, J., Ito S. (1999) Brittleness of glass. *J. Non-Cryst. Solids* **253**, 126–132.
262. Ziemath, E. C. and Herrmann, P. S. P. (2000) Densification and residual stresses induced in glass surfaces by Vickers indentations. *J. Non-Cryst. Solids* **273**, 19–24.
263. Bertoldi M., Sglavo V. M. (2004) Soda-borosilicate glass: normal or anomalous behavior under Vickers indentation? *J. Non-Cryst. Solids* **344**, 51–59.
264. Koike A., Tomozawa M. (2007) IR investigation of density changes of silica glass and sodalime silicate glass caused by microhardness indentation. *J. Non-Cryst. Solids* **353**, 2318–2327.
265. Gross, T. M. and Tomozawa, M. (2008) Indentation-induced microhardness changes in glasses: possible fictive temperature increase caused by plastic deformation. *J. Non-Cryst. Solids* **354**, 4056–4062.
266. Gross, T. M. and Tomozawa, M. (2008) Crack-free high-load Vickers indentation of silica glass. *J. Non-Cryst. Solids* **354**, 5567–5569.
267. Kato, Y., Yamazaki, H., Yoshida, S. and Matsuoka, J. (2010) Effect of densification on crack initiation under Vickers indentation test. *J. Non-Cryst. Solids* **356**, 1768–1773.
268. Perriot, A., Barthel, E., Kermouche, G., Quérel, C. and Vandembroucq, D. (2011) On the plastic deformation of sodalime glass: a Cr^{3+} luminescence study of densification. *Philos. Mag.* **91**, 1245–1255.
269. Gadeirab, K. R., Bonilla, F. A. and Chiesa, M. (2012) Densification modeling of fused silica under nanoindentation. *J. Non-Cryst. Solids* **358**, 392–398.
270. Hermansen, C., Matsuoka, J., Yoshida, S., Yamazaki, H., Kato, Y. and Yue, Y. Z. (2013) Densification and plastic deformation under microindentation in silicate glasses and the relation to hardness and crack resistance. *J. Non-Cryst. Solids* **364**, 40–43.
271. Matthewson, M. J. and Field, J. E. (1980) An improved strength-measurement technique for brittle materials. *J. Phys. E: Sci. Instrum.* **13**, 355–359.
272. van der Zwaag, S. and Field, J. E. (1983) Rain erosion damage in brittle materials. *Engng Fract. Mech.* **17**, 367–379.
273. Hutchings, I. M. (2000) Solid particle erosive wear testing. In: ASM Handbook. Vol. 8: Mechanical Testing and Evaluation, H. Kuhn, D. Medlin (eds). ASM International, Materials Park, Ohio: 338–345.
274. Sargent, G. A., Mehrotra, P. K. and Conrad, H. (1979) Multiparticle erosion of Pyrex glass. In: Erosion: Prevention and Useful Applications (*ASTM STP* 664), W. F. Adler (ed). American Society for Testing and Materials, Philadelphia: 77–100.
275. Mehrotra, P. K., Sargent, G. A. and Conrad, H. (1982) A computer simulation of the time dependence of the erosion of Pyrex glass by glass beads. *J. Mater. Sci.* **17**, 1049–1058.
276. Ritter, J. E., Strzepa, P. and Jakus, K. (1984) Erosion and strength degradation in soda-lime glass. *Phys. Chem. Glasses* **25**, 159–162.
277. Ritter, J. E., Strzepa, P., Jakus, K., Rosenfield, L. and Buckman, K. J. (1984) Erosion damage in glass and alumina. *J. Amer. Ceram. Soc.* **67**, 769–774.
278. Buijs, M. and Pasmans, J. M. M. (1995) Erosion of glass by alumina particles: transitions and exponents. *Wear* **184**, 61–65.
279. Ballout, Y., Mathias, J. A. and Talia, J. E. (1996) Solid particle erosion mechanism in glass. *Wear* **196**, 263–269.
280. Verspui, M. A., Slikkerveer, P. J., Skerka, G. J. E., Oomen, I. and de With, G. (1998) Validation of the erosion map for spherical particle impacts on glass. *Wear* **215**, 77–82.
281. Bouten, P. C. P., Scholten, H. F. and Pourreuix, C. (1999) The strength of glass sheets perforated by erosion. *Wear* **233**, 515–522.
282. Ismail, J., Zairi, F., Nait-Abdelaziz, M., Bouzid, S. and Azari, Z. (2011) Experimental and numerical investigations on erosion damage in glass by impact of small-sized particles. *Wear* **271**, 817–826.
283. Bouzid, S. and Azari, Z. (2012) Impact depth on glass surface caused by sand particles. *Appl. Mech. Mater.* **146**, 197–212.
284. Zhong, Z. W. and Han, Z. Z. (2002) Turning of glass with abrasive waterjet. *Mater. Manuf. Processes* **17**, 339–349.
285. Zhu, H. T. and Huang, C. Z. (2008) Machinability of glass by abrasive waterjet. *Int. J. Mater. Product Technol.* **31**, 106–112.
286. Matsumara, T., Muramatsu, T., Fueki, S. and Hoshi, T. (2011) Abrasive waterjet machining of glass with stagnation effect. *Ann. CIRP* **60**, 355–358.
287. Dadkhahipour, K., Nguyen, T. and Wang, J. (2012) Mechanisms of channel formation on glasses by abrasive waterjet milling. *Wear* **292**, 1–10.
288. Pang, K. L., Nguyen, T. and Fan, J. M., Wang J. (2012) A study of micro-channeling on glasses using an abrasive slurry jet. *Machining Sci. Technol.* **16**, 547–563.

© 2013 Wiley Publishing Ltd |
doi: 10.1111/str.12075

289. Wiederhorn, S. M. and Lawn, B. R. (1979) Strength degradation of glass impacted with sharp particles. 1: Annealed surfaces. *J. Amer. Ceram. Soc.* **62**, 66–70.
290. Wiederhorn, S. M., Lawn, B. R. and Hockey, B. J. (1979) Effect of particle impact angle on strength degradation of glass. *J. Amer. Ceram. Soc.* **62**, 639–640.
291. Vedder, J. F. and Mandeville, J.-C. (1974) Microcraters formed in glass by projectiles of various densities. *J. Geophys. Res.* **79**, 3247–3256.
292. Titov, V. M. (1976) Damage produced in glass by meteorite impact. *J. Appl. Mech. Tech. Phys.* **17**, 557–560.
293. Cour-Palais, B. G. (1987) Hypervelocity impact in metals, glass and composites. *Int. J. Impact. Engng* **5**, 221–238.
294. Alwes, D. (1990) Columbus-viewport glass pane hypervelocity impact testing and analysis. *Int. J. Impact Engng* **10**, 1–22.
295. Wiedlocher, D. E., Tucker, D. S., Nichols, R. and Kinser, D. L. (1992) Low-Earth-orbit effects on strength of glass. *J. Amer. Ceram. Soc.* **75**, 2893–2895.
296. Bernhard, R. P. and Christiansen, E. (1996) Analysis of microstructures and projectile residues in hypervelocity impacts on fused silica glass. In: Shock Compression of Condensed Matter 1995, S. C. Schmidt and W. C. Tao (eds). American Institute of Physics, Woodbury, New York: 1151–1154.
297. Taylor, E. A. and McDonnell, J. A. M. (1997) Hypervelocity impact on soda lime glass: damage equations for impactors in the 400–2000 μm range. *Adv. Space Res.* **20**, 1457–1460.
298. Taylor, E. A., Hayhurst, C. J. and Tsembelis, K. (1997) Hydrocode modelling of space debris hypervelocity impact on sodalime glass using the Johnson–Holmquist brittle material model. In: Proc. Second European Conference on Space Debris, B. Kaldeich-Schürmann and B. Harris (eds). European Space Agency, Noordwijk, The Netherlands: 449–453.
299. Burchell, M. J. and Grey, I. D. S. (2001) Oblique hypervelocity impacts on thick glass targets. *Mater. Sci. Engng A* **303**, 134–141.
300. McDonnell, J. A. M., Catling, D. J., Herbert, M. K. and Clegg, R. A. (2001) Quastistatic to hypervelocity impactor loading of glass: AUTODYN hydrocode and static testing configurations. *Int. J. Impact Engng* **26**, 497–496.
301. Kadono, T. and Fujiwara, A. (2005) Cavity and crater depth in hypervelocity impact. *Int. J. Impact Engng* **31**, 1309–1317.
302. Tanabe, Y. and Yasuda, E. (2005) Damage behavior of ceramic materials by impact. *J. Ceram. Soc. Jpn* **113**, 198–209.
303. Zhang, W., Ha, Y., Guan, G. and Pang, B. (2005) Experimental and numerical studies of laminated glass subject to hypervelocity impact. In: Proc. Fourth European Conference on Space Debris, D. Danesy (ed). ESA Publications Division, Noordwijk, The Netherlands: 431–436.
304. Tsembelis, K., Burchell, M. J., Cole, M. J. and Margaritis, N. (2008) Residual temperature measurements of light flash under hypervelocity impact. *Int. J. Impact Engng* **35**, 1368–1373.
305. Yang, J., Zhang, J., Gong, Z. and Pang, H. (2010) Damage analysis for hypervelocity impact experiments on spaceship windows glass. *EPJ Web Conferences* **6**, 39001.
306. Holmström, E., Samela, J. and Nordlund, K. (2011) Atomistic simulations of fracture in silica glass through hypervelocity impact. *Europhys. Letts* **96**, 16005.
307. Anderson Jr., C. E. and Holmquist, T. J. (2013) Computational modeling of failure for hypervelocity impacts into glass targets. *Procedia Engng* **58**, 194–203.
308. Song, L. H., Wei, Q., Bai, Y. and Gao, C. (2013) Impact effects on fused quartz glass by ground simulating hypervelocity space debris. *Science China: Technol. Sci.* **56**, 724–731.
309. Roybal, R., Tlomak, P., Stein, C. and Stokes, H. (1999) Simulated space debris impact experiments on toughened laminated thin solar cell cover glass. *Int. J. Impact Engng* **23**, 811–822.
310. Davison, D., Cour-Palais, B., Quan, X., Holmquist, T. J., Cohen, L. M., Ramsey, R. and Cummings, R. (2003) Computer models of micrometeoroid impact on fused silica glass mirrors. *Int. J. Impact Engng* **29**, 203–214.
311. Moussi, A., Drolshagen, G., McDonnell, J. A. M., Mandeville, J.-C., Kearsley, A. T. and Ludwig, H. (2005) Hypervelocity impacts on HST solar arrays and the debris and meteoroids populations. *Adv. Space Res.* **35**, 1243–1253.
312. Huang, J., Han, J., Li, H., Cai, M., Li, X. and Gao, Z. (2010) Study of space microimpacts on solar cells and evaluation of resultant degradation. *J. Spacecraft Rockets* **47**, 380–383.
313. Lee, N., Close, S., Goel, A., Lauben, D., Linscott, I., Johnson, T., Strauss, D., Bugiel, S., Mocker, A. and Srama, R. (2013) Theory and experiments characterizing hypervelocity impact plasmas on biased spacecraft materials. *Phys. Plasmas* **20**, 032901.
314. Mandeville, J.-C. and Vedder, J. F. (1971) Microcraters formed in glass by low density projectiles. *Earth Planet. Sci. Letts* **11**, 297–306.
315. Neukum, G., Mehl, A., Fechtig, H. and Zähringer, J. (1970) Impact phenomena of micrometeorites on lunar surface material. *Earth Planet. Sci. Letts* **8**, 31–35.
316. Walters, W. P. and Zukas, J. A. (1989) Fundamentals of Shaped Charges. John Wiley & Sons, Chichester, UK.
317. Dawes, A. P. L. (2003) The capability of glass shaped charge liners in improvised explosive devices. MSc thesis, Univ. of Cranfield, UK.
318. Baker, E. L., DeFisher, S., Daniels, A., Vuong, T., Pham, J. (2011) Glass as a shaped charge liner material. In: Proc. 26th Int. Symp. on Ballistics, E. Baker and D. Templeton (eds). Destech Publications, Lancaster, PA: 340–347.
319. Cowan, K. G. and Bourne, B. (2004) Oxide glasses as shaped charge liners. In: Proc. 21st Int. Symp. on Ballistics. SAPMEA Conventions, Wayville, South Australia, 713–720.
320. Edwards, M., Harries, R. and Henderson, E. (2008) Preliminary results from firings of glass shaped charge jets into steel targets. In: S. Bless and J. Walker (eds) Proc. 24th Int. Symp. on Ballistics. DEStech Publications Inc., Lancaster, PA: 862–869.
321. Grady, D. E. (1996) Shock-wave properties of brittle solids. In: Shock Compression of Condensed Matter 1995, S. C. Schmidt and W. C. Tao (eds). American Institute of Physics, Woodbury, New York: 9–20.
322. Church, P. D., Andrews, T. and Goldthorpe, B. (1999) A review of constitutive model development within DERA. In: Structures under Extreme Loading Conditions (*PVP* 394), D. M. Jerome (ed). American Society of Mechanical Engineers, New York: 113–120.
323. Church, P., Goldthorpe, B., Cullis, I., Rosenfeld, D. (2001) Development and validation of a dwell model. In: Proc. 19th

© 2013 Wiley Publishing Ltd | *Strain* (2014) **50**, 470–500
doi: 10.1111/str.12075

Int. Symp. on Ballistics, I. R. Crewther (ed). RUAG Land Systems, Interlaken, Switzerland: 1337–1344.
324. Holmquist, T. J. and Johnson, G. R. (2011) A computational constitutive model for glass subjected to large strains, high strain rates and high pressures. *Trans. ASME: J. Appl. Mech.* **78**, 051003.
325. Chocron, S., Dannemann, K. A., Walker, J. D., Nicholls, A. E. and Anderson, Jr. C. E. (2007) Constitutive model for damaged borosilicate glass under confinement. *J. Amer. Ceram. Soc.* **90**, 2549–2555.
326. Chocron, S., Anderson, Jr. C. E., Nicholls, A. E. and Dannemann, K. A. (2010) Characterization of confined intact and damaged borosilicate glass. *J. Amer. Ceram. Soc.* **93**, 3390–3398.
327. Chocron, S., Anderson, Jr. C. E., Dannemann, K. A. and Nicholls, A. E. (2013) Pressure effects on the compressive response of confined intact and damaged sodalime glass. *Exper. Mech.* **53**, 77–89.
328. Dannemann, K. A., Chocron, S., Nicholls, A. E. and Anderson, Jr. C. E. (2008) Compressive damage development in confined borosilicate glass. *Mater. Sci. Engng A* **478**, 340–350.
329. Grujicic, M., Pandurangan, B., Coutris, N., Cheeseman, B. A., Fountzoulas, C., Patel, P., Templeton, D. W. and Bishnol, K. D. (2009) A simple ballistic material model for sodalime glass. *Int. J. Impact Engng* **36**, 386–401.
330. Grujicic, M., Pandurangan, B., Bell, W. C., Coutris, N., Cheeseman, B. A., Fountzoulas, C., Patel, P., Templeton, D. W. and Bishnoi, K. D. (2009) An improved mechanical material model for ballistic sodalime glass. *J. Mater. Engng Perform.* **18**, 1012–1028.
331. Forde, L. C., Proud, W. G., Walley, S. M., Church, P. D. and Cullis, I. G. (2010) Ballistic impact studies of a borosilicate glass. *Int. J. Impact Engng* **37**, 568–578.
332. Dannemann, K. A., Anderson, Jr. C. E., Chocron, S. and Spencer, J. F. (2012) Damage development in confined borosilicate and sodalime glasses. *J. Amer. Ceram. Soc.* **95**, 721–729.
333. Grady, D. E., Hollenbach, R. E., Schuler, K. W. and Callender, J. F. (1977) Strain rate dependence in dolomite inferred from impact and static compression tests. *J. Geophys. Res.* **82**, 1325–1333.
334. Mott, N. F. (1943) Fragmentation of HE shells: a theoretical formula for the distribution of weights of fragments. Report No. AC3642, London, Ministry of Supply. Publ. in [338], 227–241.
335. Mott, N. F. (1943) A theory of the fragmentation of shells and bombs. Report No. AC4035, London, Ministry of Supply. Publ. in [338], 243–294.
336. Mott, N. F. (1947) Fragmentation of shell cases. *Proc. R. Soc. Lond. A* **189**, 300–308.
337. Mott, N. F. (1948) Fracture of metals: Theoretical considerations. *Engineering* **165**, 16–18.
338. Grady, D. E. (2006) Fragmentation of Rings and Shells: The Legacy of N.F. Mott. Springer, Berlin.
339. Grady, D. E. (1981) Application of survival statistics to the impulsive fragmentation of ductile rings. In: M. A. Meyers and L. E. Murr (eds) Shock Waves and High Strain Rate Phenomena in Metals. Plenum, New York: 181–192.
340. Grady, D. E. (1981) Fragmentation of solids under impulsive stress loading. *J. Geophys. Res.* **86**, 1047–1054.
341. Grady, D. E., Wilson, L. T., Reedal, D. R., Kuhns, L. D., Kipp, M. E. and Black, J. W. (2001) Comparing alternate approaches in the scaling of naturally fragmenting munitions. In: Proc. 19th Int. Symp. on Ballistics, I. R. Crewther (ed). RUAG Land Systems, Interlaken, Switzerland: 591–597.
342. Grady D. E. (2011) Impact breach and fragmentation of glass plate. *Int. J. Impact Engng* **38**, 446–450.
343. Kipp, M. E., Grady, D. E. and Chen, E. P. (1980) Strain-rate dependent fracture initiation. *Int. J. Fract.* **16**, 471–478.
344. Kipp, M. E. and Grady, D. E. (1985) Dynamic fracture growth and interaction in one dimension. *J. Mech. Phys. Solids* **33**, 399–415.
345. Grady, D. E. and Kipp, M. E. (1985) Mechanisms of dynamic fragmentation: factors governing fragment size. *Mech. Mater.* **4**, 311–320.
346. Grady, D. E. and Kipp, M. E. (1985) Geometric statistics and dynamic fragmentation. *J. Appl. Phys.* **58**, 1210–1222.
347. Johnson, G. R. and Holmquist, T. J. (1992) A computational constitutive model for brittle materials subjected to large strains, high strain rates and high pressures. In: M. A. Meyers, L. E. Murr and K. P. Staudhammer (eds) Shock-wave and High-strain-rate Phenomena in Materials. Marcel-Dekker, New York: 1075–1082.
348. Johnson, G. R. and Holmquist, T. J. (1994) An improved computational constitutive model for brittle materials. In: S. C. Schmidt, J. W. Shaner, G. A. Samara and M. Ross (eds) High Pressure Science and Technology 1993. American Institute of Physics, New York: 981–984.
349. Holmquist, T. J., Templeton, D. W. and Bishnoi, K. D. (2001) Constitutive modeling of aluminum nitride for large strain, high strain rate, and high pressure applications. *Int. J. Impact Engng* **25**, 211–231.
350. Grady, D. E. and Kipp, M. E. (1979) Oil shale fracture and fragmentation at higher rates of loading. In: Proc. 20th US Symp. on Rock Mechanics. Univ. of Austin, Austin, Texas, 403–406.
351. Grady, D. E. and Kipp, M. E. (1987) Dynamic rock fragmentation. In: Fracture Mechanics of Rock, B. K. Atkinson (ed). Academic, San Diego: 429–475.
352. Grady, D. E. (2010) Fragmentation of ceramics in the ballistic environment. *Ceram. Engng Sci. Proc.* **30**(5), 3–18.
353. Rosenberg, Z., Brar, N. S. and Bless, S. J. (1988) Elastic precursor decay in ceramics as determined with manganin strain gauges. *J. Phys. France* **49**(C3), 707–712.
354. Yaziv, D., Yeshurun, Y., Partom, Y. and Rosenberg, Z. (1988) Shock structure and precursor delay in commercial alumina. In: Shock Waves in Condensed Matter 1987, S. C. Schmidt, N. C. Holmes (eds). North Holland, Amsterdam: 297–300.
355. Murray, N. H., Bourne, N. K. and Rosenberg, Z. (1996) Precursor decay in several aluminas. In: Shock Compression of Condensed Matter 1995, S. C. Schmidt and W. C. Tao (eds). American Institute of Physics, Woodbury, New York: 491–494.

© 2013 Wiley Publishing Ltd

356. Murray, N. H., Bourne, N. K. and Rosenberg, Z. (1998) The dynamic compressive strength of aluminas. *J. Appl. Phys.* **84**, 4866–4871.
357. Drucker, D. C. and Prager, W. (1952) Soil mechanics and plastic analysis of limit design. *Quart. Appl. Math.* **10**, 157–165.
358. Heyman, J. (1972) Coulomb's Memoir on Statics: An Essay in the History of Civil Engineering. Cambridge University Press, Cambridge, 113–115.
359. Porter, D. (1995) Group Interaction Modelling of Polymer Properties. Marcel Dekker, New York.
360. Porter, D. and Gould, P. J. (2009) Predictive nonlinear constitutive relations in polymers through loss history. *Int. J. Solids Structures* **46**, 1981–1993.
361. Blumenfeld, R. and Edwards, S. F. (2009) On granular stress statistics: compactivity, angoricity, and some open issues. *J. Phys. Chem. B* **113**, 3981–3987.
362. Blumenfeld, R., Jordan, J. F. and Edwards, S. F. (2012) Interdependence of the volume and stress ensembles and equipartition in statistical mechanics of granular systems. *Phys. Rev. Letts* **109**, 238001.

© 2013 Wiley Publishing Ltd
doi: 10.1111/str.12075